Journal of Marine Engineering & Technology

Multi-objective Optimization on Steady-state Thermodynamic Parameters of S-CO2 Recompression Brayton Cycle Power Generation System for Marine Waste Heat Recovery

--Manuscript Draft--

Full Title:	Multi-objective Optimization on Steady-state Thermodynamic Parameters of S-CO2 Recompression Brayton Cycle Power Generation System for Marine Waste Heat Recovery
Manuscript Number:	TMAR-2020-0118R1
Article Type:	Original Article
Keywords:	S-CO2 recompression Brayton cycle; main engine exhaust gas; waste heat recovery; multi-objective optimization; decision making
Abstract:	Analysis of thermodynamic parameters' effects on the S-CO2 recompression Brayton cycle for recovering the main engine exhaust gas waste heat of an ocean-going 9000 TEU container ship are carried out first in this paper. NSGA-II algorithm-based multi-objective optimizations are conducted to maximize net power output and exergetic efficiency as well as to minimize the levelized cost of energy (LCOE). The final optimal result from Pareto front solutions is decided by decision-making processes. The results show that the LCOE increases along with the enhancement of net power output and exergetic efficiency, and the maximal objectives always appear near the upper boundary of exhaust gas temperature. The final optimal result decided by TOPSIS decision-making has higher rationality and accuracy than that obtained by LINMAP method. Regarding the final optimal results of triple-objective and dual-objective optimizations obtained by TOPSIS method, the former achieved more reasonable results, since its optimal net power output and exergetic efficiency are 1.29% and 5.11% higher than the latter, while its LCOE increased by 2.28% as a result of the increase of the net power output. The recompression Brayton cycle is better for recovering the exhaust gas waste heat in ships compared with the simple recuperative cycle without recompression.
Order of Authors:	Pengcheng Pan, PhD candidate
	Chengqing Yuan, PhD
	Yuwei SUN, Ph.D.
	Xinping Yan, PhD
	Mingjian Lu, PhD
	Richard Bucknall, PhD
Response to Reviewers:	List of Responses Note: Revised portions are marked in red in the manuscript. The main corrections and the responds to the reviewers' comments are as follows: Reviewer #1: This is a well written article. I would recommend it to be accepted, subject to minor comments below. (1) Is the fig. 1 derived by the authors? If not, permission to publish this figure in this journal should be seeked. Same comment applies to other figures. Responds: Thanks for the reviewer's suggestion. The data in Fig.1 was quoted from the published research papers include Singh et al. 2016, Yuan et al. 2018 and Shu et al.2017, but it was plotted by us. And, all the other figures in the whole paper were plotted by us. (2) Moroz et al. (Moroz et al. 2015) - just mention Moroz et al. (2015). You don't have to mention the name twice. Responds: Thanks for the reviewer's suggestion. We have revised all similar references in the paper according to the reviewer's comments. For example, "Tian et

al. (Tian et al. 2017) presented a systematic multi-objective optimization by GA to optimize the key parameters of carbon dioxide transcritical power cycles to ensure that the system can generate power efficiently and economically."

(3) It was interesting to observe that the LCOE is exponentially increasing with Wnet and hex for the solutions on pareto front. To what would you attribute that?
Responds: Thanks for the reviewer's comments. If the system net power output Wnet needs to be further improved, the heat exchanger area per unit power APR will increase significantly, resulting in the increasing of the structural size of the whole system and the increasing of the cost of the whole system.

(4) Pls provide in a short paragraph in conclusions recommendations for future research.
Responds: Thanks for the reviewer's suggestion. A short paragraph in conclusions recommendations for future research was added in the part of Conclusions.
Conclusions recommendations: In this study, the working fluid CO_2 in the system is considered to be always in the supercritical state. However, considering that when the system is shut down and restarted, some of the remaining working fluid CO_2 in the system may not be in its supercritical state. Thus, the influence of the transcritical CO_2 on performance of S-CO_2 recompression Brayton cycle system needs to be further studied.

Reviewer #2: 1- Section 4.2.2, paragraph 1, line 23-24
(1) More clarification needed on the obtained results of TOPSIS and LINMAP. provide an illustration on the mathematical calculations
Responds: Thanks for the reviewer's suggestion. Actually, the obtained results of TOPSIS and LINMAP in section 4.2.2, paragraph 1, line 23-24 were calculated by the deviation index Rd, calculated as:
(19)
Table 7
Multi-objective optimization results by using LINMAP and TOPSIS decision makings.
ParametersIdeal pointNadir pointLINMAPTOPSIS
Wnet (kW)313.30107.50261.50272.20
ηex (%)40.1913.4033.7135.04
LCOE ($/kWh)0.01080.03000.02050.0219
x0.990.100.670.72
mt (kg/s)11.9912.0011.9912.00
Tg (K)733.05732.79732.76732.53
Deviation index 0.25170.1997

Fig.12. The pareto front curve of triple-objective for the presented system.
The deviation index calculation method of the TOPSIS and LINMAP was based on the formula (19).
As can be seen from Fig 12 and Table 7, fj_LINMAP=268.7, fj_TOPSIS=272.20, fjideal=313.3, fjnadir=107.5. So, the deviation index of the TOPSIS and LINMAP methods were calculated as:
Rd_LINMAP=0.2517;
Rd_TOPSIS=0.1997.

(2) References number 12 & 13 need to be distinguished intext as they appear as same (name and year), however, they are different.
Responds: Thanks for the reviewer's suggestion. We changed the quotation form of Reference 13 (Crespi et al. 2017) to (Sánchez D et al. 2017).
"So far, as a result of the development in the research areas of the turbomachinery and the heat exchanger, S-CO_2 cycles have been successfully applied in the terrestrial power generation industry examples being concentrating solar power generation (Crespi Sánchez et al. 2017; Binotti et al. 2017; Polimeni et al. 2018; Belmonte et al. 2016; Al-Sulaiman et al. 2015), next-generation nuclear reactors (Dostal et al. 2004) and industrial waste heat recovery systems (Li et al. 2017; Yoon et al. 2017)]".

Table

Table 1

Principal data of the ocean-going 9000 TEU container ship.

Items	Characteristics	Values
Principal dimension	Length (m)	300
	Moulded Breadth (m)	48.2
	Deadweight/DWT (t)	73125
	Voyage speed (kn)	21.5
Main engine	Engine type	8S90ME-C10.2
	Speed at MCR_{ME} (r/min)	84.0
	MCR_{ME} (kW)	41900
	SFC_{ME} at 75% MCR (g/kWh)	159.61
	SFC_{AE} (g/kWh)	185
	P_{AE} (kW)	1435.75
	Exhaust temperature before turbocharger (℃)	460
	Exhaust temperature after turbocharger (℃)	270
	Exhaust mass flow rate (kg/s)	52.1
	Exhaust gas pressure (MPa)	0.308

Table 2

The equations for different components of S-CO_2 recompression Brayton cycle.

Components	Energetic equations	Exergetic equations
Main compressor	$\eta_{isen,mc}=(h_{2s}-h_1)/(h_2-h_1)$	$I_{mc}=W_{mc}-(E_2-E_1)$
	$W_{mc}=m(h_2-h_1)$	$\eta_{ex,mc}=(E_2-E_1)/W_{mc}$
Recompression compressor	$\eta_{isen,rec}=(h_{10s}-h_9)/(h_{10}-h_9)$	$I_{rec}=W_{rec}-(E_{10}-E_9)$
	$W_{rec}=m(h_{10}-h_9)$	$\eta_{ex,rec}=(E_{10}-E_9)/W_{rec}$
HTR	$\varepsilon_{HTR}=(T_7-T_8)/(T_7-T_4)$	$I_{HTR}=E_7-E_8-(E_5-E_4)$
	$Q_{HTR}=m(h_5-h_4)=m(h_8-h_7)$	$\eta_{ex,HTR}=(E_5-E_4)/(E_7-E_8)$
LTR	$Q_{LTR}=m(h_3-h_2)=m(h_9-h_8)$	$I_{LTR}=E_8-E_9-(E_3-E_2)$
		$\eta_{ex,LTR}=(E_3-E_2)/(E_8-E_9)$
Turbine	$\eta_{isen,t}=(h_6-h_7)/(h_6-h_{7s})$	$I_t=E_6-E_7-W_t$
	$W_t=m(h_6-h_7)$	$\eta_{ex,t}=W_t/(E_6-E_7)$
Gas heat exchanger	$Q_{in}=m(h_6-h_5)$	$I_{hxr}=E_{gas,in}+E_5-E_{gas,out}-E_6$
		$\eta_{ex,hxr}=(E_6-E_5)/(E_{gas,in}-E_{gas,out})$
Pre-cooler	$Q_{prc}=m(h_9-h_1)$	$I_{prc}=E_{prc,in}+E_{water,in}-E_{prc,out}-E_{water,out}$
		$\eta_{ex,prc}=(E_{prc,out}-E_{prc,in})/(E_{water,in}-E_{water,out})$

Table 3

Economic data and cost function C_i for the proposed system.

System component	Unit	Cost functions
Main compressor	USD	$71.1 \cdot m_{mc} \cdot (1/0.92-\eta_{mc}) \cdot p_r \cdot \ln(p_r)$
Re-compressor	USD	$71.1 \cdot m_{rc} \cdot (1/0.92-\eta_{rc}) \cdot p_r \cdot \ln(p_r)$
Turbine	USD	$479.34 \cdot m_t \cdot (1/0.93-\eta_t) \cdot \ln(p_r) \cdot (1+\exp(0.036 \cdot T_{t\_in}-54.4))$
Precooler	USD	$2143 \cdot A^{0.514}_{PRC}$
HTR	USD	$2681 \cdot A^{0.514}_{HTR}$
LTR	USD	$2681 \cdot A^{0.514}_{LTR}$
Exhaust gas heat exchanger	USD	$2681 \cdot A^{0.514}_{hxr}$
Maintenance and operation factor	%	6.0

Table 4

Calculation results in the present paper compared with Ref. [37].

$T_{mc,in}$ (℃)	m_t (kg/s) Ref.	m_t (kg/s) Present	*RD* (%)	η_{th} (%) Ref.	η_{th} (%) Present	*RD* (%)
32	98.50	97.69	0.83	47.40	47.00	0.84
50	134.20	134.16	0.03	41.80	41.52	0.67

Table 5

Thermodynamic parameters and their initial values for system thermodynamic analysis and performance multi-objective optimization.

Parameters	Values
Ambient temperature (℃)	21
Ambient pressure (MPa)	0.1
Isentropic efficiency of the turbine (%)	70-80
Isentropic efficiency of the main compressor (%)	60-70
Isentropic efficiency of the re-compressor (%)	60-70
Pinch point temperature difference of LTR (℃)	5
Pinch point temperature difference of HTR (℃)	8
Flow split ratio	0.4
LTR effectiveness (%)	90
HTR effectiveness (%)	89

Table 6

Thermodynamic parameters for performance multi-objective optimization.

Parameters	Values
Main compressor inlet temperature (℃)	34
Main compressor inlet pressure (MPa)	8.0
Pressure ratio	2.5
Turbine inlet temperature (℃)	420
Turbine isentropic efficiency (%)	75
Re-compressor isentropic efficiency (%)	65
Main compressor isentropic efficiency (%)	65

Table 7

Multi-objective optimization results by using LINMAP and TOPSIS decision makings.

Parameters	Ideal point	Nadir point	LINMAP	TOPSIS
W_{net} (kW)	313.30	107.50	261.50	272.20
η_{ex} (%)	40.19	13.40	33.71	35.04
LCOE ($/kWh)	0.0108	0.0300	0.0205	0.0219
x	0.99	0.10	0.67	0.72
m_t (kg/s)	11.99	12.00	11.99	12.00
T_g (K)	733.05	732.79	732.76	732.53
Deviation index			0.2517	0.1997

Table 8

Comparison between optimal solutions for dual-objective (W_{net}-*LCOE*) optimization.

Decision makings		Design variables			Objectives		Deviation index
		x	m_t (kg/s)	T_g (K)	W_{net} (kW)	*LCOE* ($/kWh)	
NSGA-II	LINMAP	0.67	11.99	732.76	259.90	0.0203	0.2595
	TOPSIS	0.70	11.99	733.15	268.70	0.0214	0.2167

Table 9

Comparison between optimal solutions for dual-objective (η_{ex} -*LCOE*) optimization.

Decision makings		Design variables			Objectives		Deviation index
		x	m_t (kg/s)	T_g (K)	η_{ex} (%)	*LCOE* ($/kWh)	
NSGA-II	LINMAP	0.68	11.99	733.12	33.25	0.0200	0.2605
	TOPSIS	0.66	12.00	733.14	33.01	0.0190	0.2693

Table 10

Comparison between optimal solutions for dual-objective (W_{net}-η_{ex}) optimization.

	Decision makings	Design variables			Objectives		Deviation index
		x	m_t (kg/s)	T_g (K)	W_{net} (kW)	η_{ex} (%)	
NSGA-II	LINMAP						
	TOPSIS	0.99	11.99	733.05	313.30	40.19	0

Figure

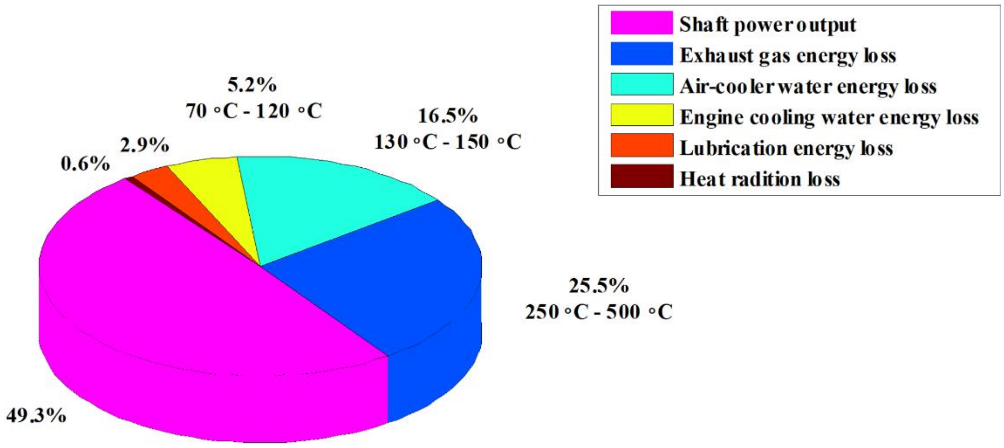

Fig.1. Energy balance of a large-scale low-speed two-stroke marine diesel engine.

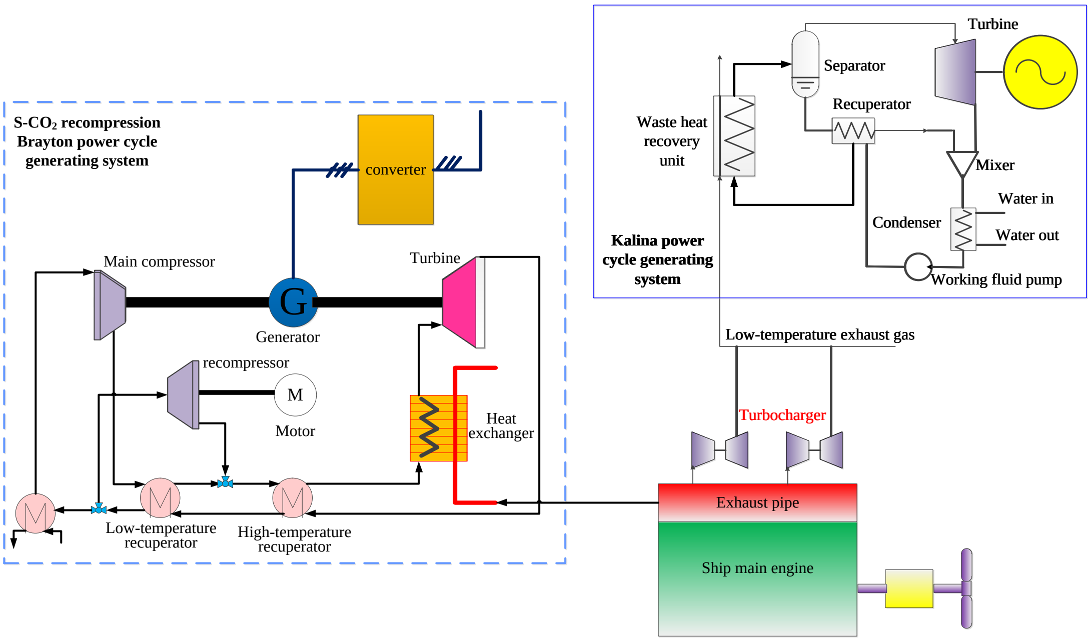

Fig.2. The general schematic diagram of the combined new power cycle generation system.

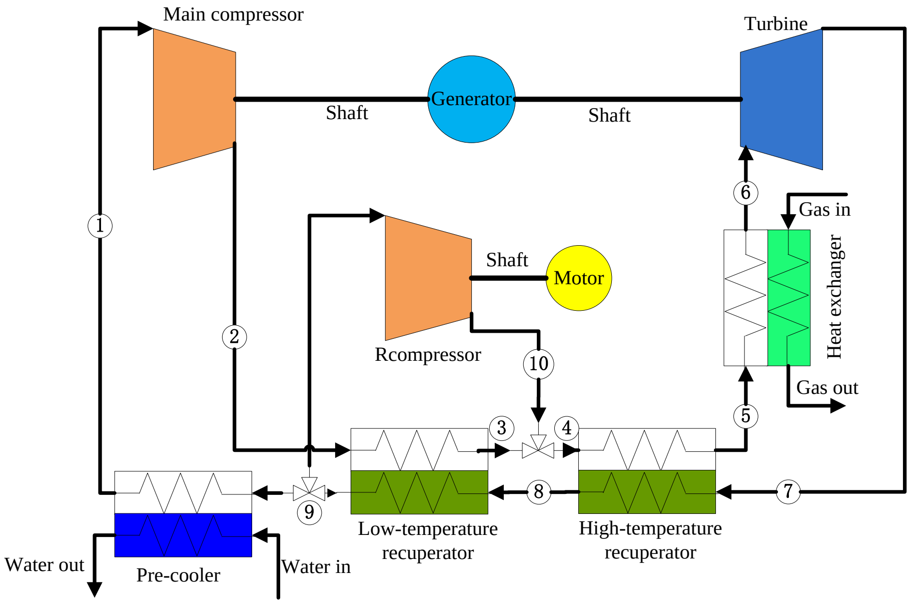

Fig.3. The system configuration of the S-CO_2 recompression Brayton power cycle.

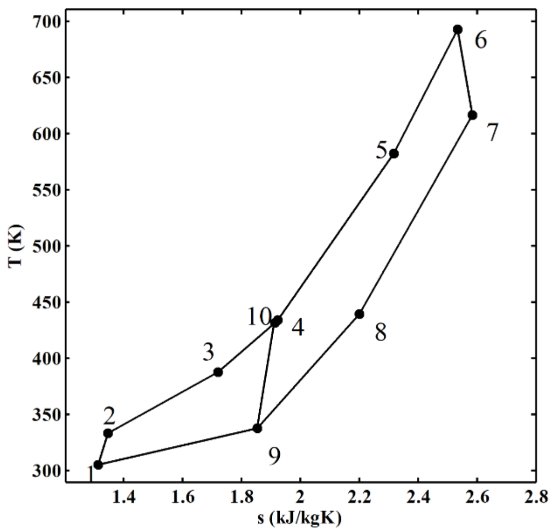

Fig. 4. *T-s* diagram of the S-CO_2 recompression Brayton power cycle.

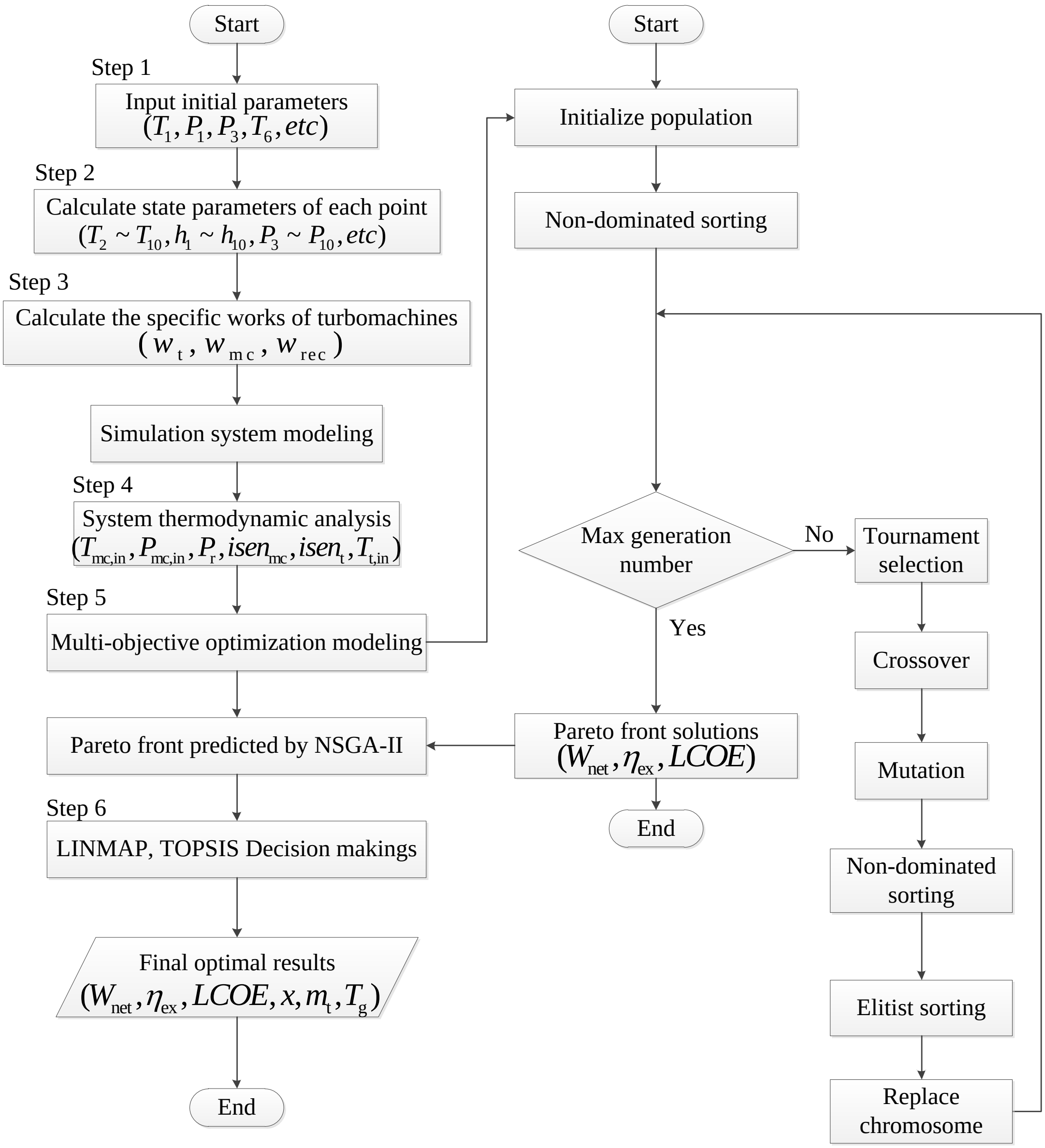

Fig.5. Flow chart of the thermodynamic analysis and parametric optimization.

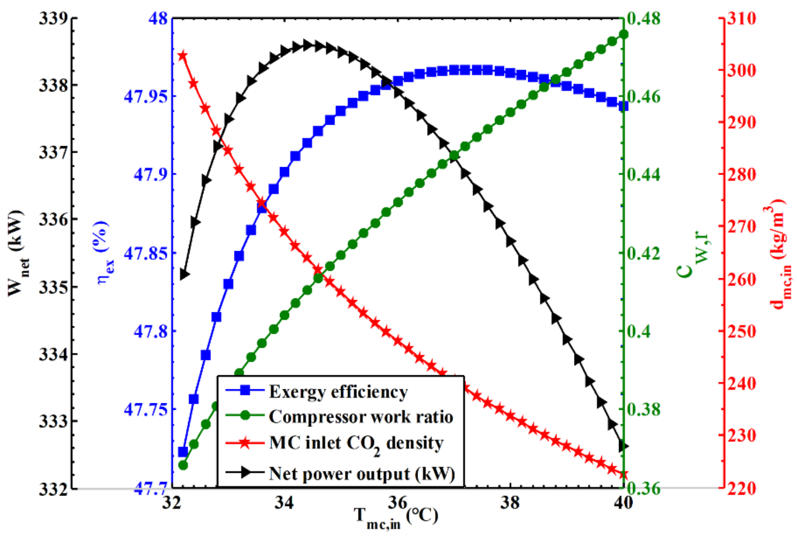

Fig. 6. Variations in different parameters with main compressor inlet temperature.

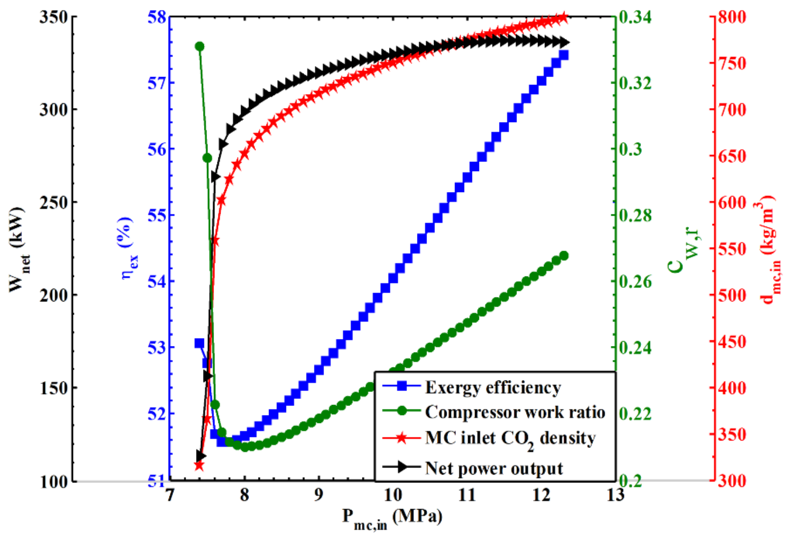

Fig. 7. Variations in different parameters with main compressor inlet pressure.

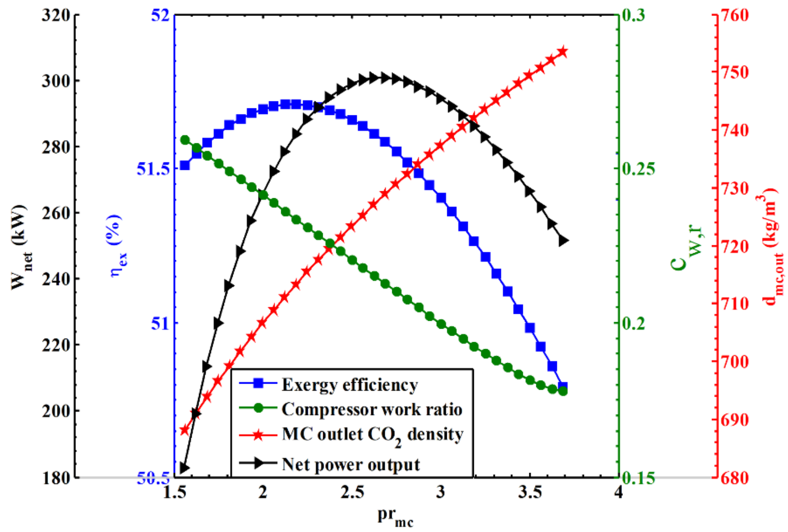

Fig. 8. Variations in different parameters with pressure ratio.

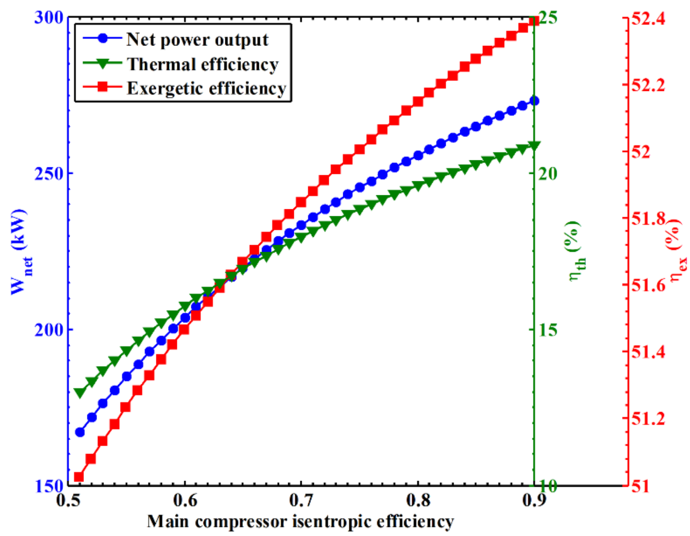

Fig. 9. Variations in system net power output, thermal efficiency and exergetic efficiency with main compressor isentropic efficiency.

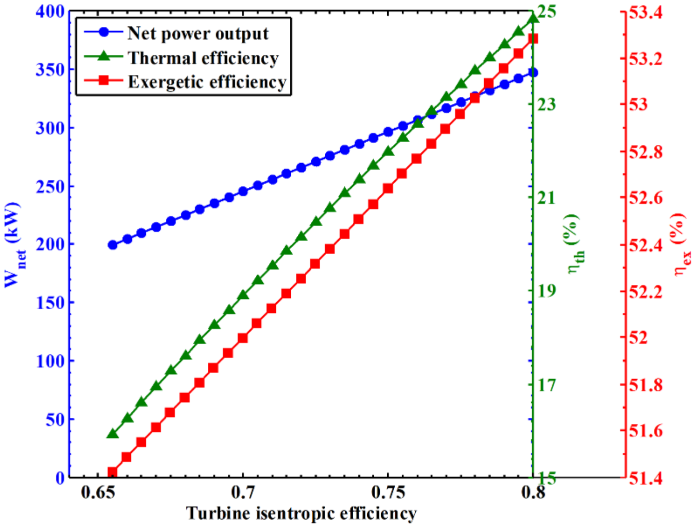

Fig. 10. Variations in system net power output, thermal efficiency and exergetic efficiency with turbine isentropic efficiency.

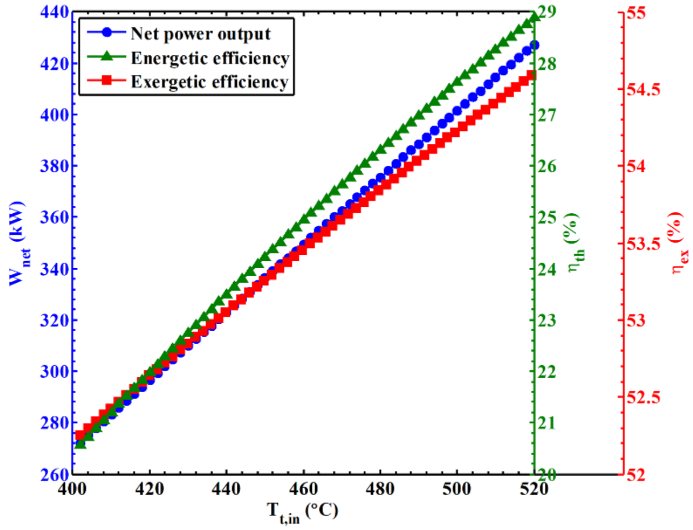

Fig. 11. Variations in system net power output, thermal efficiency and exergetic efficiency with turbine inlet temperature.

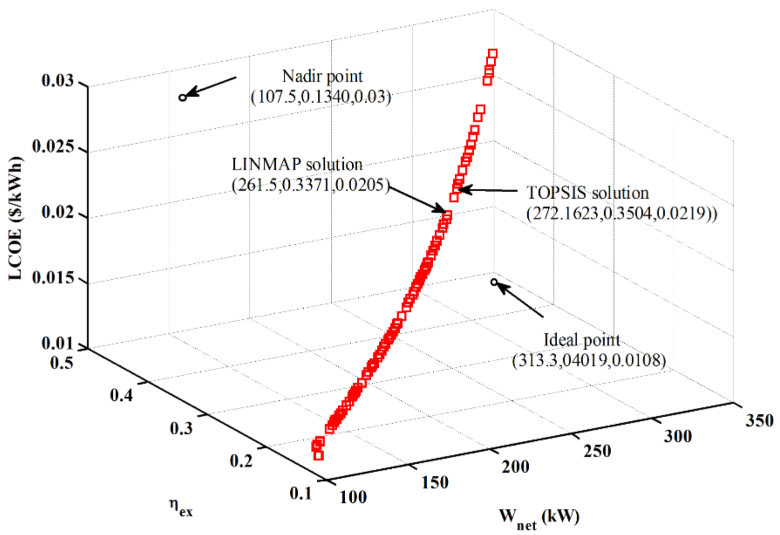

Fig.12. The pareto front curve of triple-objective for the presented system.

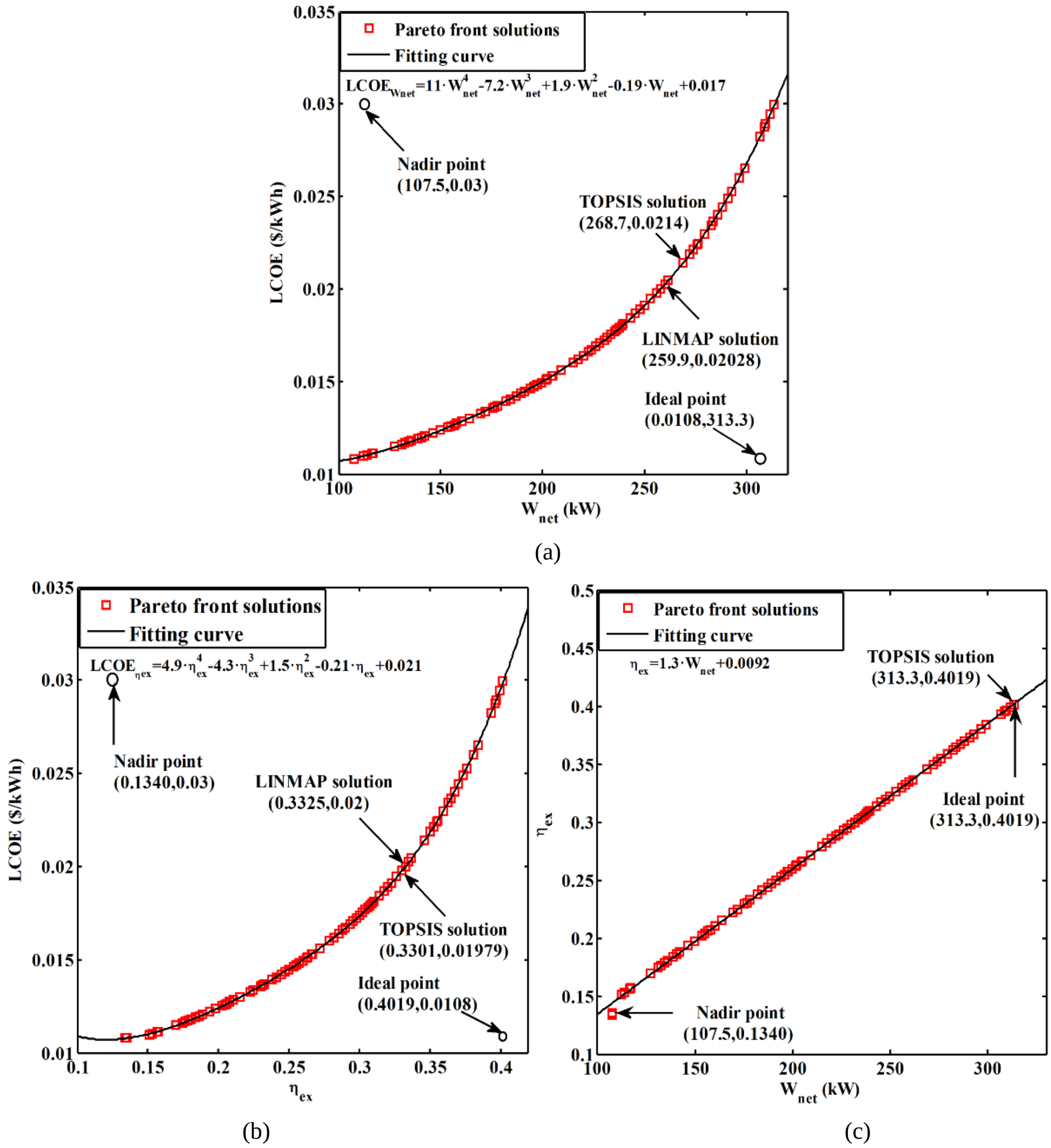

Fig.13. Pareto front solutions fitting curves: (a). Net power output and levelized cost of energy; (b). Exergetic efficiency and levelized cost of energy; (c). Net power output and exergetic efficiency.

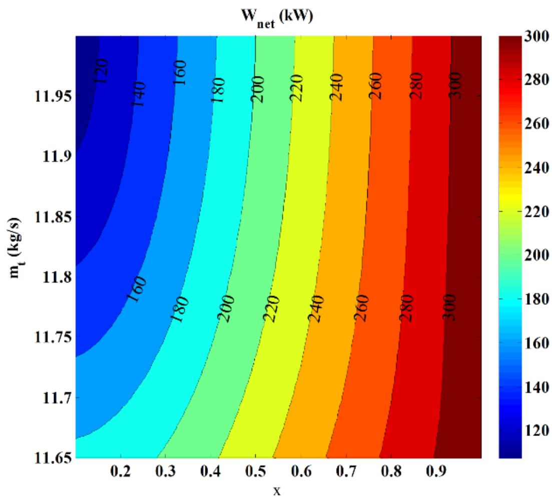

(a)

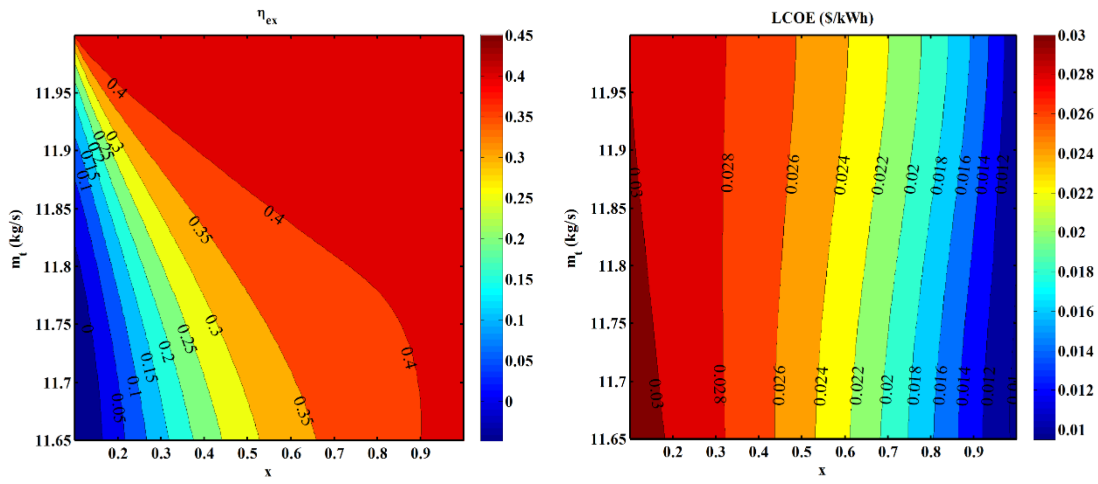

(b) (c)

Fig.14. Objectives variations with mass flow rate and flow split ratio: (a). Net power output; (b). Exergetic efficiency; (c). Levelized cost of energy.

Multi-objective Optimization on Steady-state Thermodynamic Parameters of S-CO_2 Recompression Brayton Cycle Power Generation System for Marine Waste Heat Recovery

Pengcheng PAN[1,2,4],Chengqing YUAN[1,2,3], Yuwei SUN[1,2,3*], Xinping YAN[1,2,3], Mingjian Lu[1,2,3], Richard Bucknall[4]

1. School of Energy and Power Engineering, Wuhan University of Technology, Wuhan, Hubei Province 430063, China; 2. Reliability Engineering Institute, National Engineering Research Center for Water Transport Safety (WTS Center, MoST), Wuhan University of Technology, Wuhan, Hubei Province 430063, China; 3. Key Laboratory of Marine Power Engineering & Technology (MoT), Wuhan University of Technology, Wuhan, Hubei Province 430063, China; 4. Department of Mechanical Engineering, University College London, London, UK.

Abstract

Analysis of thermodynamic parameters' effects on the S-CO_2 recompression Brayton cycle for recovering the main engine exhaust gas waste heat of an ocean-going 9000 TEU container ship are carried out first in this paper. NSGA-II algorithm-based multi-objective optimizations are conducted to maximize net power output and exergetic efficiency as well as to minimize the levelized cost of energy (LCOE). The final optimal result from Pareto front solutions is decided by decision-making processes. The results show that the LCOE increases along with the enhancement of net power output and exergetic efficiency, and the maximal objectives always appear near the upper boundary of exhaust gas temperature. The final optimal result decided by TOPSIS decision-making has higher rationality and accuracy than that obtained by LINMAP method. Regarding the final optimal results of triple-objective and dual-objective optimizations obtained by TOPSIS method, the former achieved more reasonable results, since its optimal net power output and exergetic efficiency are 1.29% and 5.11% higher than the latter, while its LCOE increased by 2.28% as a result of the increase of the net power output. The recompression Brayton cycle is better for recovering the exhaust gas waste heat in ships compared with the simple recuperative cycle without recompression.

Keywords: S-CO_2 recompression Brayton cycle; main engine exhaust gas; waste heat recovery; multi-objective optimization; decision making

[*] Corresponding Author: Yuwei Sun, 1985-, PhD, Associate professor, Research interests: renewable energy application technology, electric power system and automation, system modeling and simulation.

Nomenclature

E	exergy, kJ/kg	hxr	gas heat exchanger
h	specific enthalpy, kJ/kg	isen	isentropic
I	exergy destruction, kW	in	input
m	mass flow rate, kg/s	mc	main compressor
P	pressure, MPa	net	net power output, kW
Q	heat transfer rate, kW	out	output
s	specific entropy, kJ/kgK	prc	pre-cooler
T	temperature, K	r	ratio
W	power, kW	rec	recompression compressor
w	specific work, kW	t	turbine
LCOE	Levelized cost of energy ($/kWh)	th	thermal efficiency
Greek symbols		0	ambient condition
η	efficiency	1-10	state points
ε	recuperator effectiveness	2s, 7s, 10s	outlet isentropic enthalpy states
Subscripts		**Abbreviations**	
ex	exergetic efficiency	HTR	high-temperature recuperator
g	exhaust gas	LTR	low-temperature recuperator
		S-CO_2	Supercritical CO_2
		TEU	Twenty-foot Equivalent Unit

1. Introduction

Shipping is one of the most critical modes of transportation for world trade and accounts for approximately 90% of the global trade (Poulsen et al. 2016; Yuan et al. 2019). The global shipping industry is also one of the main contributors to global greenhouse gas (GHG) emissions, with it currently being responsible for about 3% of the global total (Lee et al. 2013). To restrict and lower the level of GHG emissions from the operation of newly-built ships, the International Maritime Organization (IMO) has formulated regulations such as the Energy Efficiency Design Index (EEDI) and the Ship Energy Efficiency Management Plan (SEEMP) (Beşikci et al. 2016; Perera et al. 2016). In today's global shipping industry, the diesel engine, which relies on fossil fuels, is still the most widely used power plant. However, its average energy efficiency is less than 50%, meaning that more than half of the input thermal energy cannot be exploited. Fig.1 shows the energy balance of a typical large low-speed two-stroke marine diesel engine and the main waste heat sources, temperature ranges and thermal energy loss rates (Singh et al. 2016; Yuan et al. 2018;

Shu et al. 2017). It can be seen that heat energy loss from the exhaust gas is the bulk of the energy dissipation, which accounts for about 25.5% of the total input fuel thermal energy. This is followed by the air cooler (16.5%), jacket cooling water (5.2%), lubricating oil (2.9%) and heat radiation (0.6%).

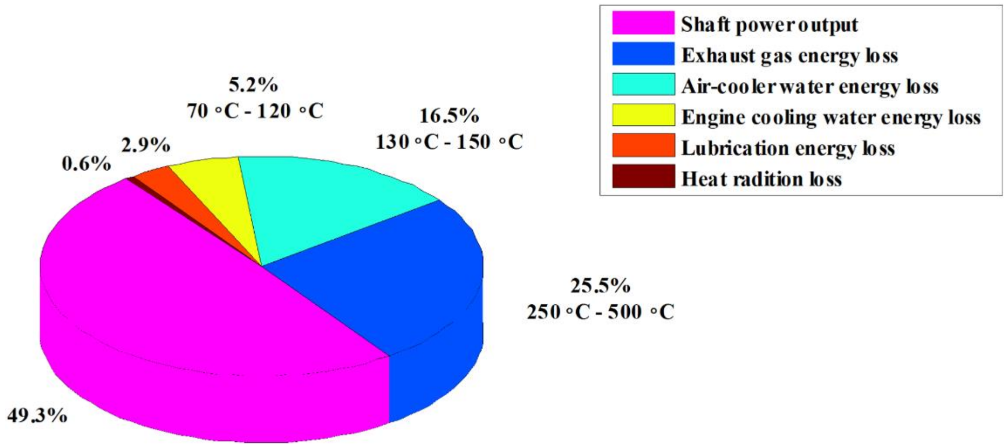

Fig.1. Energy balance of a large-scale low-speed two-stroke marine diesel engine.

From Fig.1, the exhaust gas temperature ranges from 250 ℃ to 500 ℃ under normal working conditions. Therefore, the main engine exhaust gas waste heat energy is worth recovering when considering its quality and quantity of heat energy. The commonly used technology to recover the main engine exhaust gas waste heat in a ship is the combined turbocharger and exhaust gas boiler (EGB) system. In this combined waste heat recovery system, the exhaust gas temperature at the outlet of the turbocharger is still relatively high (220 ℃~240 ℃) in the first conversion stage, so there is potential for further exploitation of this energy source (Yuan et al. 2018). So, the EGB is used as the second stage heat utilization equipment to recover the exhaust gas waste heat energy after the turbocharger. However, from the point view of the thermodynamic exergy analysis, the aforementioned technology cannot make full use of the exhaust gas waste heat. To further improve the utilization rate of the exhaust gas waste heat, alternative power cycle waste heat recovery technologies could offer promising options such as the Organic Rankine cycle (ORC), Rankine cycle (RC) and supercritical CO_2 (S-CO_2) cycle.

Considering the limited available space and the special working conditions in a ship, the exhaust gas temperature range, operational safety and cost, the S-CO_2 cycle offers significant potential to recover the ship main engine exhaust gas waste heat owing to its advantages of a stable and non-toxic working fluid, compactness of size, relatively high efficiency and lower cost (Crespi et al. 2017).

The first proposed S-CO_2 cycle was a partial condensation Brayton cycle patented by Sulzer in the late 1940s (1950). During the 1960s, Feher (1968) and Angelino (1968) contributed to some breakthroughs in the research field of the S-CO_2 cycle. Since then, the S-CO_2 cycle continued to develop and has derived various layouts such as inter-cooling, inter-recuperation reheating, pre-compression, partial cooling and preheating (Dostal 2004). Dostal (2004) proposed the S-CO_2 RBC and Kulhánek et al. (2011) proved it has the highest efficiency and best performance over other S-CO_2 cycles. So far, as a result of the development in the research areas of the turbomachinery and the heat exchanger, S-CO_2 cycles have been successfully applied in the terrestrial power generation industry examples being concentrating solar power generation (Sánchez et al. 2017; Binotti et al. 2017; Polimeni et al. 2018; Belmonte et al. 2016; Al-Sulaiman et al. 2015), next-generation nuclear reactors (Dostal et al. 2004) and industrial waste heat recovery systems (Li et al. 2017; Yoon et al. 2017).

Apart from the research into the application of S-CO_2 cycles in terrestrial power generation industries, study on introducing S-CO_2 cycles into ships to recover the main engine waste heat has also been carried out. Moroz et al. (2015) studied the performance of a combined S-CO_2 and a conventional steam cycle to recover a shipboard gas turbine and found that the net power output increased by about 30%. Bella (2015) analyzed the performance of the S-CO_2 Brayton power cycle to recover the ship's gas turbine exhaust gas waste heat, which can lower the fuel consumption by about 22%. Sharma et al. (2017) conducted the parametric optimization of a S-CO_2 regenerative recompression Brayton power cycle to recover a ship's gas turbine exhaust gas waste heat and it was found that the overall energy system efficiency and net power output increased by 10% and 25%, respectively. Hou et al. (2017) stated that the S-CO_2 regenerative recompression cycle system could be used as the backup generator because it can meet 80% of the propulsion power demand of the ship when the gas turbine fails. Furthermore, Choi (2016) studied the thermodynamic performance of a transcritical CO_2 heat recovery system with a 2-stage reheat to recover the internal combustion engine cooling water waste heat in a 6800 TEU container ship. The aforementioned research has proved that the S-CO_2 cycle can be used as waste heat recovery systems in ships to contribute to the goal of energy-saving and emissions reduction in the shipping industry.

Since 2017, researchers from Wuhan University of Technology have devoted themselves to the study of the integrated application of the S-CO_2 cycle with a Kalina cycle for recovering the main engine exhaust gas waste heat of an ocean-going 9000 TEU container ship. The principal parameters of the ship are listed in Table 1. Usually, any available space in the ship's engine room will be limited and the working environment is very harsh. It is therefore a requirement that any proposed waste heat recovery system should offer significant advantages in terms of system structural simplicity, energy efficiency, operational safety, cost and maintenance (Deng et al. 2017).

Considering the aforementioned factors, the S-CO_2 recompression Brayton cycle (S-CO_2 RBC) could be a reasonable option because it is compact with high efficiency and low cost. It can also reduce the amount of compressor work required and avoid the pinch point issue (Deng et al. 2017). Fig. 2 shows the structure diagram of the integrated S-CO_2 cycle and Kalina cycle waste heat recovery system. As shown in Fig.2, the S-CO_2 RBC system is designed to recover the high-temperature exhaust gas waste heat from the main engine exhaust gas before the turbocharger and the Kalina cycle used to convert the low-temperature exhaust gas waste heat after the turbocharger. The reason for the combination of these two cycles is to further reduce the exhaust gas outlet temperature with the overall purpose of using the waste heat in depth. The design power output of the S-CO_2 RBC waste heat recovery system is 300 kW. The expected goal of this research project is that the ship fuel consumption and the attained EEDI be decreased by at least 2% and 3%, respectively.

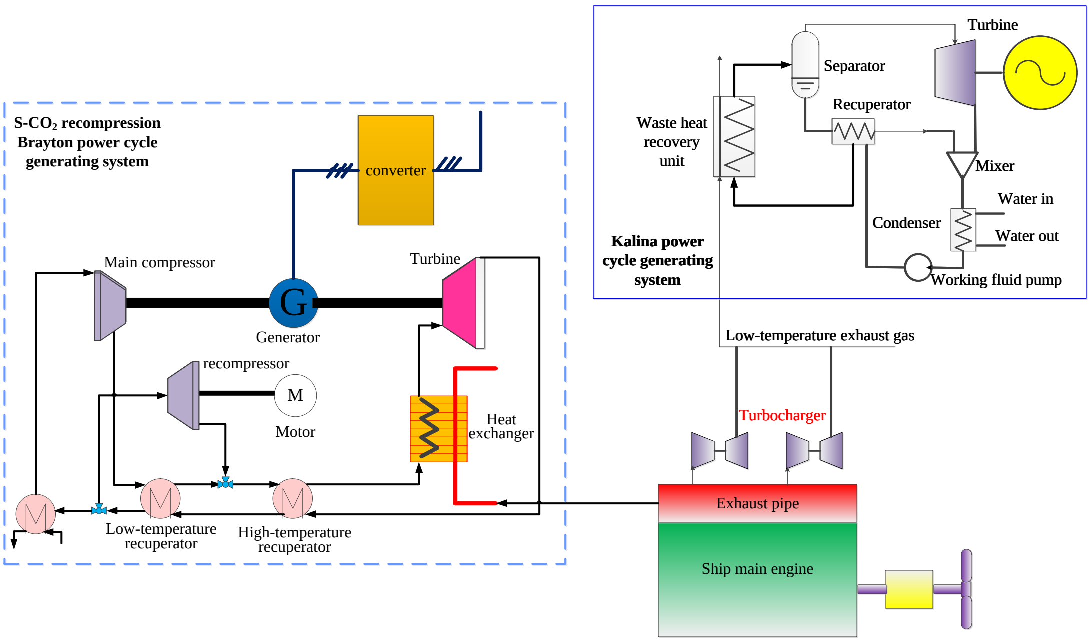

Fig.2. The general schematic diagram of the combined new power cycle generation system.

Table 1

Principal data of the ocean-going 9000 TEU container ship.

Items	Characteristics	Values
Principal dimension	Length (m)	300
	Moulded Breadth (m)	48.2
	Deadweight/DWT (t)	73125
	Voyage speed (kn)	21.5
Main engine	Engine type	8S90ME-C10.2
	Speed at MCR_{ME} (r/min)	84.0
	MCR_{ME} (kW)	41900
	SFC_{ME} at 75% MCR (g/kWh)	159.61

SFC_{AE} (g/kWh)	185
P_{AE} (kW)	1435.75
Exhaust temperature before turbocharger (°C)	460
Exhaust temperature after turbocharger (°C)	270
Exhaust mass flow rate (kg/s)	52.1
Exhaust gas pressure (MPa)	0.308

For the S-CO_2 RBC, its thermodynamic parameters can be divided into design and off-design categories (Cheng et al. 2017). Off-design parameters such as turbomachinery isentropic efficiency and pressure drop can be fixed. Design parameters such as system maximum pressure, mass flow rate and flow split ratio, need to be optimized to ensure that the system can operate safely and efficiently (Cheng et al. 2017). Therefore, for S-CO_2 cycles, study of the effects of thermodynamic parameters on system performance to decide their optimal ranges is very essential to ensure the system can deliver improved performance. Energy, Exergy and Exergoeconomic (3E) analysis methods (Wu et al. 2017) are commonly used to conduct the system thermodynamic analysis. Sharma et al. (2017) studied the effects of the turbine inlet temperature, main compressor inlet temperature, pressure ratio and pressure drop across the gas turbine on the performance of an S-CO_2 recompression Brayton power cycle waste heat recovery system. Banik et al. (2016) found that the recompression transcritical CO_2 power cycle can achieve better system performance at higher pressure ratio from 1.9 to 2.4. Furthermore, Sarkar (2009) revealed that the main compressor inlet temperature effects on optimum pressure ratio and cycle efficiency of the S-CO_2 recompression Brayton power cycle are more predominant than the maximum operating temperature. According to the previous research, it is clear that the thermodynamic parameters not only have comprehensive effects on the system performance but also interact with each other. Even though the same thermodynamic parameter will have inconsistent values for different configurations and specific applications.

To ensure that the proposed system can convert energy more efficiently and operate safely, it is critical to conduct a parametric optimization process of the system design. Artificial Neural Network (ANN), Genetic Algorithm (GA), Artificial Bee Colony (ABC) algorithm and Particle Swarm Optimization (PSO) are evolutionary algorithms used to speed up the search process for optimizing the S-CO_2 cycle system thermodynamic parameters and performance. Wang et al. (2010) optimized the simple S-CO_2 cycle turbine inlet pressure and temperature with exergy efficiency as the objective function by using ANN compared with GA. However, only optimizing single system performance indicators like exergy efficiency or thermal efficiency may not be sufficient to obtain reasonable results for system parametric optimization. Multi-objective optimization is an effective method to overcome the shortcomings of single-objective optimization.

Deng et al. (2017) conducted multi-objective optimization based on an NSGA-II algorithm to study the performance of a gas turbine S-CO_2 RBC waste heat recovery system. Tian et al. (2017) presented a systematic multi-objective optimization by GA to optimize the key parameters of carbon dioxide transcritical power cycles to ensure that the system can generate power efficiently and economically. Similar research has been carried out by using the GA (Cao et al. 2017) and ABC algorithm (Zhang et al. 2018).

The literature review reveals that the system thermodynamic parameters that have significant effects on the S-CO_2 cycle system performance need to be determined and optimized because their values are closely affected by the specific applications. Furthermore, it is a strategically convenient stage to cost effectively evaluate the system performance and economics through the system's optimal design before introducing the S-CO_2 RBC into the ship. This paper focuses on the steady-state thermodynamic analysis and performance of multi-objective optimization of the S-CO_2 RBC, when used to recover the main engine exhaust gas waste heat of an ocean-going 9000 TEU container ship. First, thermodynamic analysis is conducted to determine the variation trends of the system's performance with change of thermodynamic parameters and decide their initial values, including main compressor inlet temperature and pressure, pressure ratio, turbomachinery isentropic efficiency and turbine inlet temperature. Then, performance multi-objective including dual-objective (W_{net}-$LCOE$, η_{ex}-$LCOE$, W_{net}-η_{ex})) and triple-objective (W_{net}-$LCOE$-η_{ex}) optimizations are carried out by using the elitist non-dominated sorting genetic (NSGA-II) algorithm, using flow split ratio, turbine mass flow rate and exhaust gas waste heat temperature as decision variables. Finally, LINMAP and TOPSIS decision-making methods are employed to decide the final optimal result from the Pareto front solutions obtained by the NSGA-II algorithm.

2. System description and mathematical models

2.1. System description

The main components of the S-CO_2 RBC system are the main compressor, re-compressor, turbine, LTR, HTR and pre-cooler. The pre-cooler is deployed to ensure that the thermodynamic conditions of the working fluid CO_2 are close to its critical point before entering the main compressor. Fig.3 and Fig.4 show the system configuration diagram and its *T*-*s* diagram. In the proposed system, a splitter divides the working fluid CO_2 into two parts before entering the pre-cooler. A part of the working fluid flows into the bypass loop to be pressurized in the recompression compressor, and then joins the cold stream cycle from the entry point between the LTR and HTR. By lowering the mass flow rate through the cold side of the LTR, the bypass loop can balance the capacitance rates of the cold stream and hot stream, which results in higher efficiency compared with a simple recuperated cycle without recompression (Dyreby. 2014). In spite of the higher compression work, the thermal efficiency is improved compared to the single recuperated cycle due to the heat input at a higher temperature level and the reduction of the heat of CO_2 rejected to the ambient (Manente et al. 2019). The details of the proposed system thermodynamic processes are as follows:

Process 1-2 and 9-10: isentropic compression in the main compressor and recompression compressor.

Process 2-3 and 8-9: isobaric heat exchange between the cold working fluid and hot working fluid in the LTR.

Process 4-5 and 8-7: isobaric heat exchange between the cold working fluid and hot working fluid in the HTR.

Process 3-4 and 10: mixed flow.

Process 5-6: isobaric heat absorption process in the heat exchanger between the cold working fluid and the ship main engine exhaust gas.

Process 6-7: isentropic expansion in the turbine.

Process 9-1: heat rejection process in the pre-cooler.

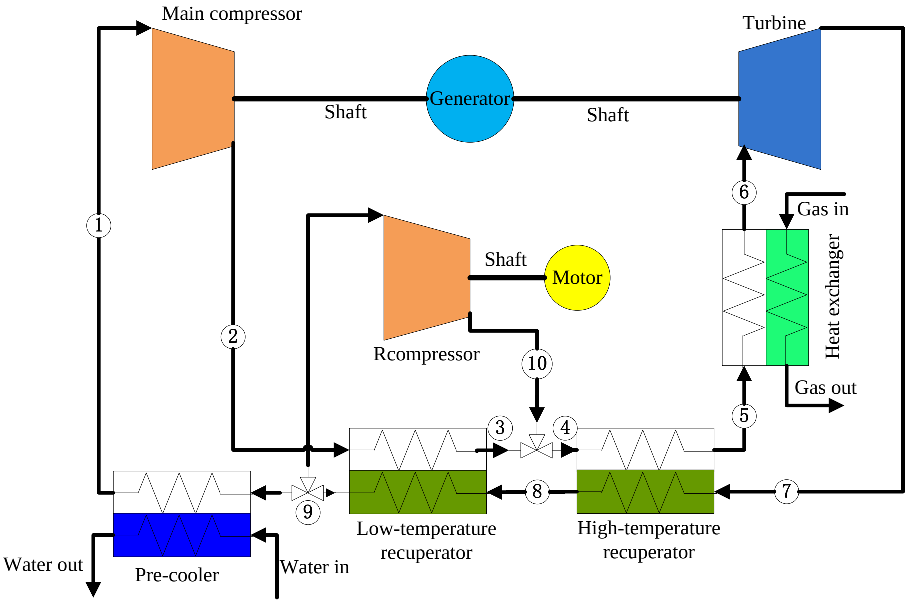

Fig.3. The system configuration of the S-CO_2 recompression Brayton power cycle.

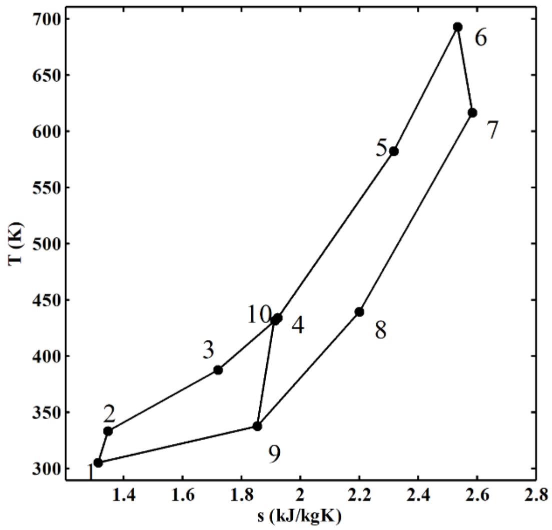

Fig. 4. *T-s* diagram of the S-CO_2 recompression Brayton power cycle.

2.2. Mathematical model

Certain assumptions are made to simplify the system thermodynamics for analysis, modeling and calculation in this work (Sarkar et al. 2009; Akbari et al. 2014).

(1) The closed-loop system operates under the steady-state condition without any leakage of the working fluid CO_2.

(2) Pressure drops and heat losses in the pipes are neglected.

(3) Only physical exergy of the working fluid CO_2 is considered, while the chemical exergy, kinetic exergy and potential exergy changes in all components are neglected.

2.2.1. Energetic analysis

The thermodynamic models of the S-CO_2 RBC main components are presented in Table 2 (Zhao et al. 2016).

The net power output W_{net} of the proposed system is defined as:

$$W_{\mathrm{net}} = W_{\mathrm{t}} - W_{\mathrm{mc}} - W_{\mathrm{rec}} \tag{1}$$

The thermal efficiency η_{th} is defined as the ratio of net power output W_{net} to the heat absorbed from the heat exchanger Q_{in}:

$$\eta_{\mathrm{th}} = \frac{W_{\mathrm{net}}}{Q_{\mathrm{in}}} \tag{2}$$

The main compressor specific work w_{mc}, re-compressor specific work w_{rec} and turbine specific work w_{t} are defined as follows:

$$w_{\mathrm{mc}} = h_2 - h_1 \tag{3}$$

$$w_{\mathrm{rec}} = h_{10} - h_9 \tag{4}$$

$$w_t = h_6 - h_7 \quad (5)$$

The LTR effectiveness depends on the heat capacity. If the heat capacity of the high-pressure fluid is greater than that of low-pressure fluid, then Eq. (6-1) is applicable. Eq. (6-2) is applicable for the reverse case (Sarkar 2009; Sarkar et al. 2009):

$$\varepsilon_{LTR} = (T_8 - T_9)/(T_8 - T_2) \quad (6\text{-}1)$$

$$\varepsilon_{LTR} = (T_3 - T_2)/(T_8 - T_2) \quad (6\text{-}2)$$

2.2.2. Exergetic analysis

The ambient environment pressure P_0 and temperature T_0 are set as the reference state values. In this study, the working fluid chemical exergy is ignored and only its physical exergy is considered. The exergy of the i_{th} steady-state point E_i can be defined as:

$$E_i = m[(h_i - h_0) - T_0(s_i - s_0)] \quad (7)$$

The component exergy loss I can be calculated by:

$$\sum E_{in} - \sum E_{out} = I \quad (8)$$

The system total exergy loss $\sum I$ is defined as:

$$\sum I = I_{hxr} + I_{prc} + I_{HTR} + I_{LTR} + I_t + I_{mc} + I_{rec} \quad (9)$$

The exergetic efficiency η_{ex} of the whole system can be calculated as:

$$\eta_{ex} = \frac{E_{in} - \sum I}{E_{in}} \quad (10)$$

The exergetic efficiency of the S-CO_2 RBC can also be defined as (Zhang et al. 2018):

$$\eta_{ex} = \frac{\eta_{th}}{(1 - T_0/T_g)} \quad (11)$$

Table 2

The equations for different components of S-CO_2 recompression Brayton cycle.

Components	Energetic equations	Exergetic equations
Main compressor	$\eta_{isen,mc}=(h_{2s}-h_1)/(h_2-h_1)$	$I_{mc}=W_{mc}-(E_2-E_1)$
	$W_{mc}=m(h_2-h_1)$	$\eta_{ex,mc}=(E_2-E_1)/W_{mc}$
Recompression compressor	$\eta_{isen,rec}=(h_{10s}-h_9)/(h_{10}-h_9)$	$I_{rec}=W_{rec}-(E_{10}-E_9)$
	$W_{rec}=m(h_{10}-h_9)$	$\eta_{ex,rec}=(E_{10}-E_9)/W_{rec}$
HTR	$\varepsilon_{HTR}=(T_7-T_8)/(T_7-T_4)$	$I_{HTR}=E_7-E_8-(E_5-E_4)$
	$Q_{HTR}=m(h_5-h_4)=m(h_8-h_7)$	$\eta_{ex,HTR}=(E_5-E_4)/(E_7-E_8)$
LTR	$Q_{LTR}=m(h_3-h_2)=m(h_9-h_8)$	$I_{LTR}=E_8-E_9-(E_3-E_2)$
		$\eta_{ex,LTR}=(E_3-E_2)/(E_8-E_9)$
Turbine	$\eta_{isen,t}=(h_6-h_7)/(h_6-h_{7s})$	$I_t=E_6-E_7-W_t$

	$W_t=m(h_6-h_7)$	$\eta_{ex,t}=W_t/(E_6-E_7)$
Gas heat exchanger	$Q_{in}=m(h_6-h_5)$	$I_{hxr}=E_{gas,in}+E_5-E_{gas,out}-E_6$
		$\eta_{ex,hxr}=(E_6-E_5)/(E_{gas,in}-E_{gas,out})$
Pre-cooler	$Q_{prc}=m(h_9-h_1)$	$I_{prc}=E_{prc,in}+E_{water,in}-E_{prc,out}-E_{water,out}$
		$\eta_{ex,prc}=(E_{prc,out}-E_{prc,in})/(E_{water,in}-E_{water,out})$

2.2.3. Economic analysis

The levelized cost of energy (LCOE, \$/kWh) defined as the average cost per unit of energy produced by the proposed system, is used to evaluate the economics of the S-CO_2 RBC waste heat recovery system in this work.

$$LCOE=\sum_{i=1}^{N}c_i/W_{net} \tag{12}$$

The cost rate for the i_{th} component c_i is calculated by considering the purchase cost, operating and maintenance cost which can be defined as follows:

$$c_i=(\frac{CRF+\gamma_k}{t})\cdot C_i \tag{13}$$

Where γ_k is the maintenance factor (0.06); t is the annual operation hours (7200 h); C_i is the initial investment component (\$); *CRF* is the capital recovery factor which can be calculated by:

$$CRF=\frac{k(1+k)^n}{(1+k)^n-1} \tag{14}$$

Where k is the interest rate (12%); n is the system operation life cycle (20 years).

To estimate the area of the heat exchangers, constant values of the overall heat transfer coefficient are introduced for the purpose of simplicity. The constant value of the LTR and exhaust gas heat exchanger is 1.6 kW/m^{2}K. The values of HTR and pre-cooler are selected as 3.0 kW/m^2 K and 2.0 kW/m^{2}K, respectively (Zhang et al. 2018). The economic data and cost functions are listed in Table 3.

Table 3
Economic data and cost function C_i for the proposed system (Zhang et al. 2018; Liu et al. 2018).

System component	Unit	Cost functions
Main compressor	USD	$71.1\cdot m_{mc}\cdot(1/0.92-\eta_{mc})\cdot p_r\cdot\ln(p_r)$
Re-compressor	USD	$71.1\cdot m_{rc}\cdot(1/0.92-\eta_{rc})\cdot p_r\cdot\ln(p_r)$
Turbine	USD	$479.34\cdot m_t\cdot(1/0.93-\eta_t)\cdot\ln(p_r)\cdot(1+\exp(0.036\cdot T_{t\_in}-54.4))$
Precooler	USD	$2143\cdot A^{0.514}{}_{PRC}$
HTR	USD	$2681\cdot A^{0.514}{}_{HTR}$
LTR	USD	$2681\cdot A^{0.514}{}_{LTR}$
Exhaust gas heat exchanger	USD	$2681\cdot A^{0.514}{}_{hxr}$

Maintenance and operation factor	%	6.0

2.3. Model validation

The relative deviation *RD* is defined as:

$$RD = \frac{|ref - rel|}{ref} \times 100\% \tag{15}$$

Where *ref* represents the reference value and *rel* is the real value calculated by the simulation model in this paper.

The verification of the model of the proposed system was conducted by comparing the turbine mass flow rate and thermal efficiency in the present paper to those in Ref. (Dyreby 2014) under the consistent initial conditions. Table 4 compares the results between the Ref. (Dyreby 2014) and the simulation model present in this study. The deviations are less than 1.0% which indicates that the proposed system thermodynamic simulation model is validated for use in this study.

Table 4
Calculation results in the present paper compared with Ref. (Dyreby 2014).

$T_{\mathrm{mc,in}}$ (℃)	m_{t} (kg/s) Ref.	m_{t} (kg/s) Present	*RD* (%)	η_{th} (%) Ref.	η_{th} (%) Present	*RD* (%)
32	98.50	97.69	0.83	47.40	47.00	0.84
50	134.20	134.16	0.03	41.80	41.52	0.67

3. Methodology

Fig.5 is the solution process flow chart of the thermodynamic analysis and parametric optimization.

(1) Input the initial parameters including main compressor inlet temperature T_1, pressure P_1 and outlet pressure P_2 as well as turbine inlet temperature T_6.

(2) Calculate the working conditions from state point 1 to state point 10, including temperatures ($T_2 \sim T_{10}$), pressures ($P_3 \sim P_{10}$), entropies ($E_1 \sim E_{10}$) and enthalpies ($h_1 \sim h_{10}$).

(3) Compute the main compressor specific work w_{mc}, re-compressor specific work w_{rec} and turbine specific work w_{t}.

(4) After completing the aforementioned steps, the whole system simulation model can be established based on the system mathematical models, and the initial values (including main compressor inlet temperature $T_{\mathrm{mc,in}}$, main compressor inlet pressure $P_{\mathrm{mc,in}}$, pressure ratio P_{r}, main compressor isentropic efficiency $isen_{\mathrm{t}}$, turbine isentropic efficiency $isen_{\mathrm{mc}}$

and turbine inlet temperature $T_{\mathrm{t,in}}$) of thermodynamic parameters that decide the system performance characteristics can be investigated through thermodynamic analysis.

(5) The NSGA-II algorithm is used to optimize the system net power output W_{net}, exergetic efficiency η_{ex} and levelized cost of energy *LCOE*, using the flow split ratio x, turbine mass flow rate m_{t} and exhaust gas waste heat temperature T_{g} as decision variables.

(6) The LINMAP and TOPSIS decision making methods are employed to select the final optimal result from the Pareto front solutions obtained by NSGA-II.

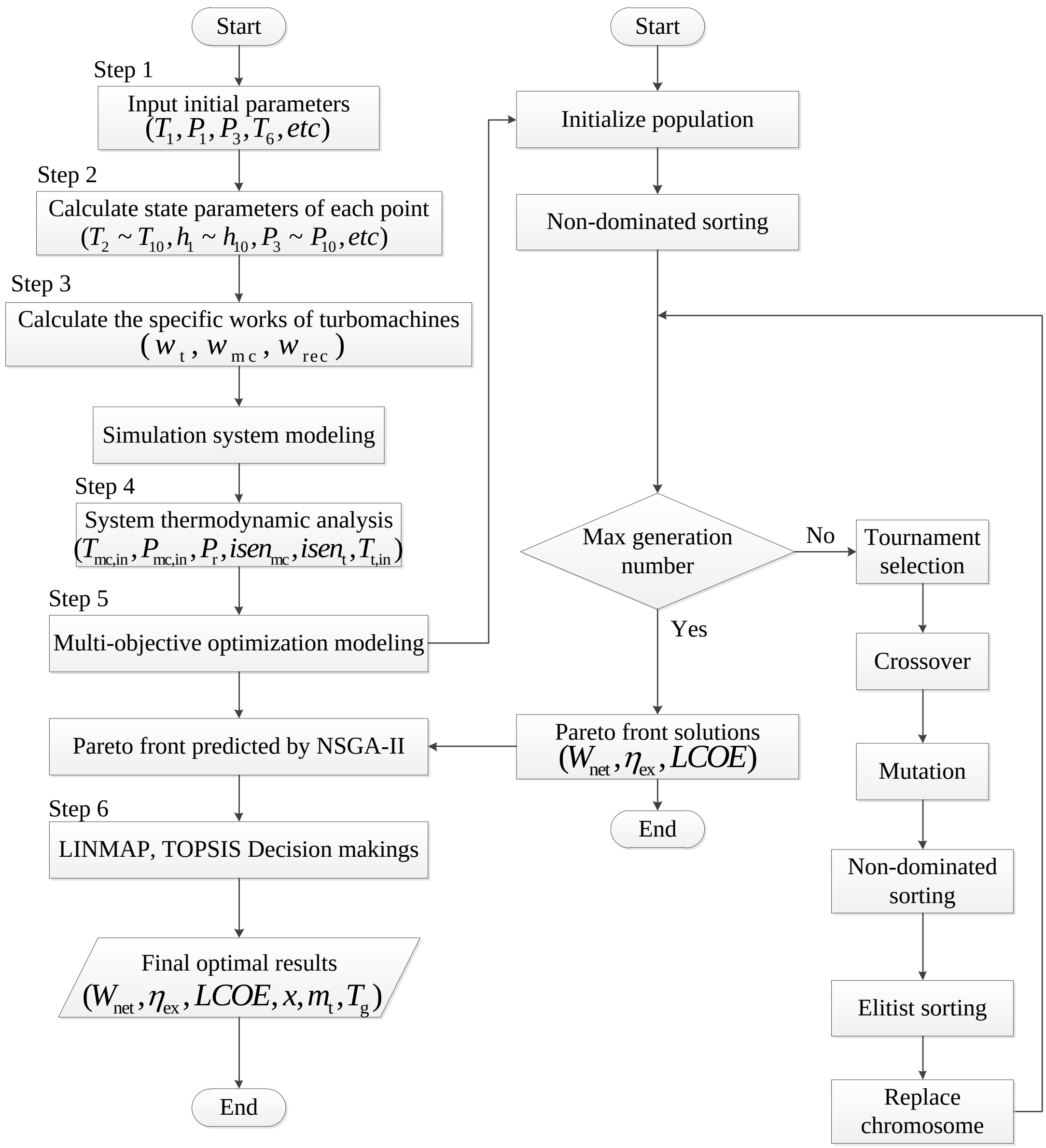

Fig.5. Flow chart of the thermodynamic analysis and parametric optimization.

3.1. NSGA-II algorithm

The NSGA-II algorithm was first proposed by Deb et al. (2002) and Shi et al. (2010) concluded that it is one of the best methods to solve multi-objective optimization issues. The algorithm calculation flow chart is shown in Fig. 5.

3.2. Decision-making process

Pareto front solutions are considered equally good in the multi-objective optimization processes. So, a final optimal solution needs to be decided from the Pareto front solutions, which is the trade-off solution between the conflict objective functions. In this study, the most recognized and common type of decision-making methods include LINMAP and TOPSIS, and are used to decide the final optimal result from the Pareto front solutions obtained by the NSGA-II algorithm.

3.2.1. LINMAP decision-making

The basic principle of the LINMAP decision-making is to calculate the Euclidean distance from each Pareto front solution to the ideal point, and the solution with the minimum distance is selected as the final optimal result (Moghimi et al. 2018). The ideal point is optimum with respect to all of the objective functions. The Euclidean distance is calculated as follows (Li et al. 2015):

$$D_{i+} = \sqrt{\sum_{j=1}^{n} (f_{ij} - f_j^{\text{ideal}})^2} \tag{16}$$

Where f_j^{ideal} is the ideal solution point of the j_{th} objective in a single-objective optimization calculation.

3.2.2 TOPSIS decision making

TOPSIS is a decision-making method which was first developed by Hwang and Yoon (1981). In TOPSIS decision-making process, the ideal point and nadir point are considered simultaneously. Therefore, the Euclidean distances of each Pareto front solution to the ideal point and the nadir point should be calculated. The Euclidian distance of each solution to the nadir point can be defined as (Li et al. 2015; Sianaki 2015):

$$D_{i-} = \sqrt{\sum_{j=1}^{n} (f_{ij} - f_j^{\text{nadir}})^2} \tag{17}$$

The maximum d_i will help to decide the final optimal solution, which is defined as follows:

$$d_i = \frac{D_{i+}}{D_{i+} + D_{i-}} \tag{18}$$

To evaluate the final optimal solutions obtained by these two decision-making methods, the deviation index *Rd* is introduced (Li et al. 2015):

$$Rd = \frac{\sqrt{\sum_{j=1}^{n} (f_j - f_j^{\text{ideal}})^2}}{\sqrt{\sum_{j=1}^{n} (f_j - f_j^{\text{ideal}})^2} + \sqrt{\sum_{j=1}^{n} (f_j - f_j^{\text{nadir}})^2}} \tag{19}$$

4. Results and discussions

4.1 Thermodynamic analysis

Both thermodynamic analysis and performance multi-objective optimization of the proposed system are conducted by simulation models established in MATLAB. The thermodynamic properties of the CO_2 are calculated based on the REFPROP (NIST standard reference database 23 2019) database developed by the National Institute of Standards and Technology of the United States.

In this work, the pressure drops of the main components and the temperature differences in the LTR and HTR can be decided based on the previous research. The pressure drops of the cold stream and hot stream in the HTR and LTR are set to 0.15 MPa and 0.08 MPa, the pressure drop values in the gas heat exchanger and pre-cooler are set to 0.08 MPa (Dyreby 2014). The effectiveness of the HTR and LTR are assumed to 95% and 89% (Park et al. 2018). Considering system operational safety and manufacturing technologies, the maximum pressure in the proposed system is set at 20 MPa. The initial values of the thermodynamic parameters to conduct thermodynamic analysis and performance multi-objective optimization are listed in Table 5.

Table 5
Thermodynamic parameters and their initial values for system thermodynamic analysis and performance multi-objective optimization.

Parameters	Values
Ambient temperature (℃)	21
Ambient pressure (MPa)	0.1
Maximum pressure (MPa)	20
HTR effectiveness (%)	93
LTR effectiveness (%)	89
Flow split ratio	0.4

4.1.1. Effects of the main compressor inlet temperature

The main compressor inlet temperature is defined as the minimum temperature in the S-CO_2 RBC system in this work. The main compressor initial inlet pressure is fixed at 7.38 MPa to analyze the effects of inlet temperature on the system performance due to the working fluid CO_2 requiring lower compression work near the critical zone (31.1 ℃, 7.38 MPa), which can contribute to the system achieve better system performance (Guo et al. 2018). The compressor work ratio is defined as the ratio of compression work (shaft power) to the turbine work (shaft work). Fig.6 shows the effects of the main compressor inlet temperature on the net power output, exergetic efficiency, compressor work ratio and the CO_2 density at the inlet of the main compressor. Fig.6

shows that the net power output continues to increase to a maximum of 338.50 kW as the inlet temperature approaches 34 ℃, and then decreases. Increasing the main compressor inlet temperature results in the reduction of the CO_2 density at the inlet of the main compressor as shown in Fig. 6. Therefore, the main compressor needs to consume more turbine output work to compress the working fluid to maintain the mass flow rate required for the turbine. Before the inlet temperature reaches 34 ℃, the system net power output increases because the turbine output shaft power increases at a higher rate than the increase in the shaft work required to drive the compressor. However, when the inlet temperature exceeds 34 ℃, incremental increase of the main compressor compression work leads to the decreasing of the net power output. To ensure the proposed system has a better performance, the main compressor inlet temperature is fixed at 34 ℃ to conduct the following analysis.

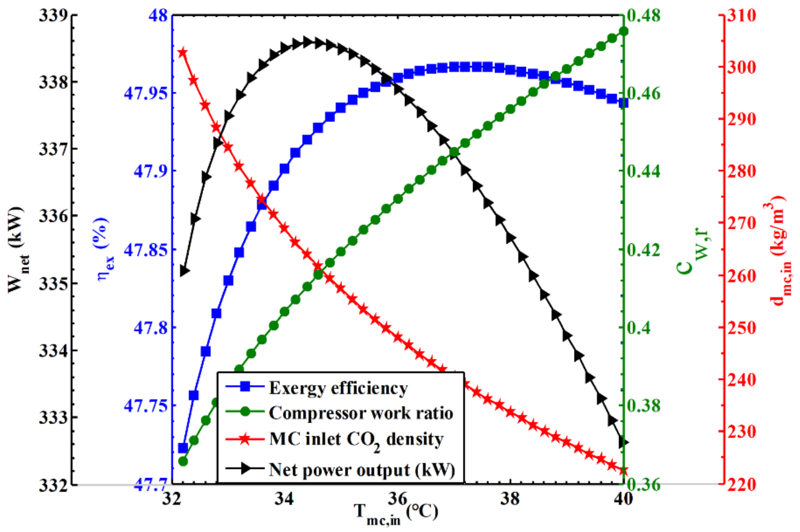

Fig. 6. Variations in different parameters with main compressor inlet temperature.

4.1.2. Effects of the main compressor inlet pressure

The main compressor inlet pressure is defined as the minimum pressure in the proposed system in this paper. As shown in Fig. 7 the main compressor inlet pressure has significant effect on the thermal properties of the working fluid CO_2, especially its density. From Fig. 7, before the inlet pressure approaches 8.0 MPa, the net power output increases sharply due to the decrease in compression work caused by the dramatic increase of CO_2 density. Then, the effect of the main compressor inlet pressure on the system net power output becomes less significant because density of the CO_2 gradually stabilizes. The values of net power output are 302.30 kW at $P_{mc,in}$ =8.0 MPa and 335.70 kW at $P_{mc,in}$ =11 MPa. Only a 9.95% average increase of the system net power output when the main compressor inlet pressure is raised by 27.27% (From 8 MPa to 11 MPa). Although the results show that a higher main compressor inlet pressure contributes to more power, higher inlet pressure in turbomachinery components requires thicker piping and casing that will cause an increase in cost (Guo et al. 2018). Therefore, considering the aforementioned reasons, the main compressor inlet pressure is fixed at 8.0 MPa.

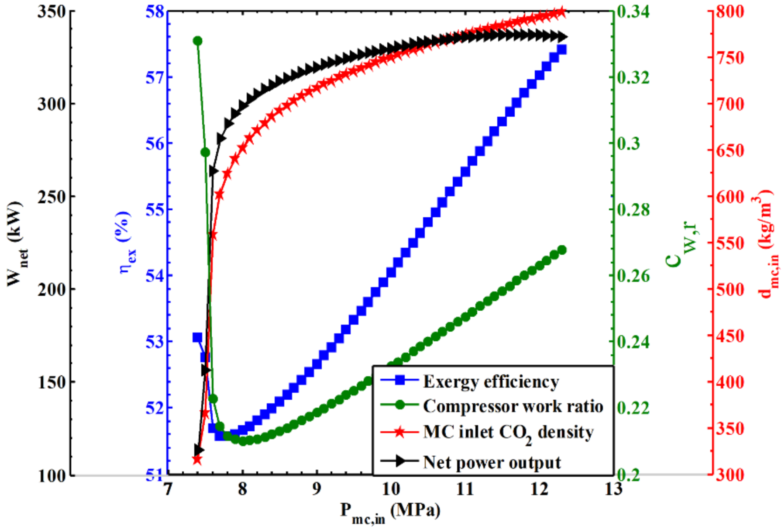

Fig. 7. Variations in different parameters with main compressor inlet pressure.

4.1.3. Effects of the pressure ratio

The pressure ratio in this study is defined as the ratio of the main compressor outlet pressure to its inlet pressure. As shown in Fig. 8, the net power output and exergetic efficiency continue to increase to a maximum, and then decrease. Each of the system performance metrics have their own optimal pressure ratio. The maximum net power output is 311.90 kW when pr_{mc} =2.7, and the corresponding exergetic efficiency is about 52.82%. If the pressure ratio is set to 2.7, then the maximum main compressor outlet pressure is 21.60 MPa, which is higher than the constraint condition of 20 MPa as mentioned above. Compared with the net power output of 309.30 kW at a pr_{mc} of 2.7, the net power output at a pr_{mc} of 2.5 only decreases by approximately 0.83%. Therefore, it is acceptable for the pressure ratio to be fixed at 2.5 in this work, which can guarantee the maximum pressure does not exceed the upper safety limit while still allowing the system to deliver improved performance.

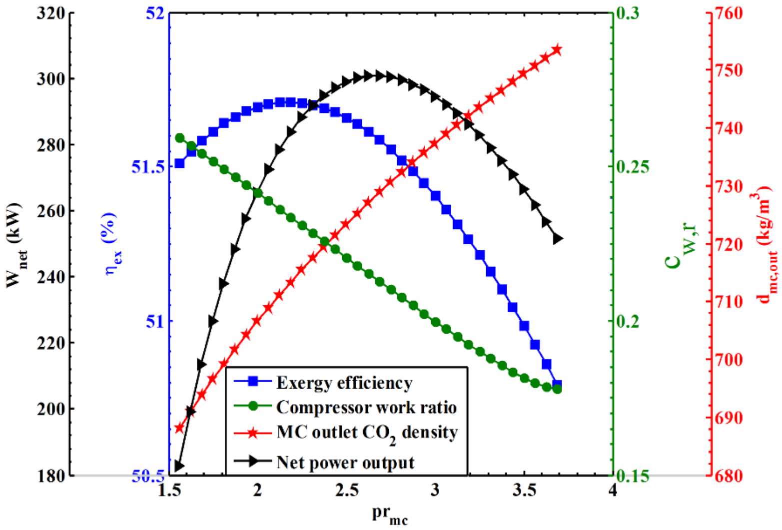

Fig. 8. Variations in different parameters with pressure ratio.

4.1.4 Effects of the main compressor isentropic efficiency

The main compressor efficiency is decided by its isentropic efficiency. Fig. 9 shows the effects of the main compressor's isentropic efficiency on system performance. As can be seen, the main compressor isentropic efficiency has a positive influence on the net power output, thermal efficiency and exergetic efficiency. If the main compressor isentropic efficiency increases by 10%, the system net power output, thermal efficiency and exergetic efficiency are raised approximately 8.51%, 8.24% and 0.46%. It is clear that the effects of the main compressor isentropic efficiency on the system performance is limited. Although higher main compressor isentropic efficiency contributes to improve the system performance, the main compressor isentropic efficiency is set to 65% when the present mechanical process technic level of the turbomachinery is taken into consideration.

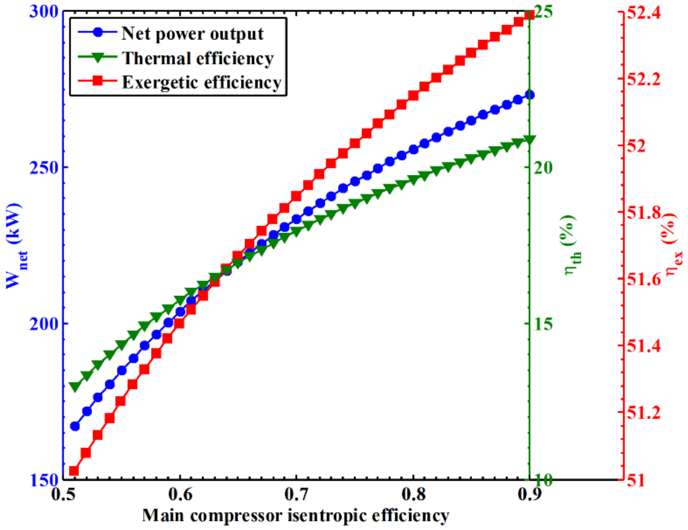

Fig. 9. Variations in system net power output, thermal efficiency and exergetic efficiency with main compressor isentropic efficiency.

4.1.5 Effects of the turbine isentropic efficiency

The turbine's isentropic efficiency determines its mechanical efficiency, which has a direct effect on the system net power output because the turbine output shaft power is used to drive the generator. Fig.10 shows the effects of the turbine isentropic efficiency on the system performance. The system net power output, thermal efficiency and exergetic efficiency all increase linearly with increase of the turbine isentropic efficiency. It is clear that the turbine's isentropic efficiency has greater effect on the system performance compared with that of the main compressor. Higher turbine isentropic efficiency leads to increased power and improves the system energy efficiency. The turbine isentropic efficiency is taken to be 75% in this study owing to current manufacturing limitations.

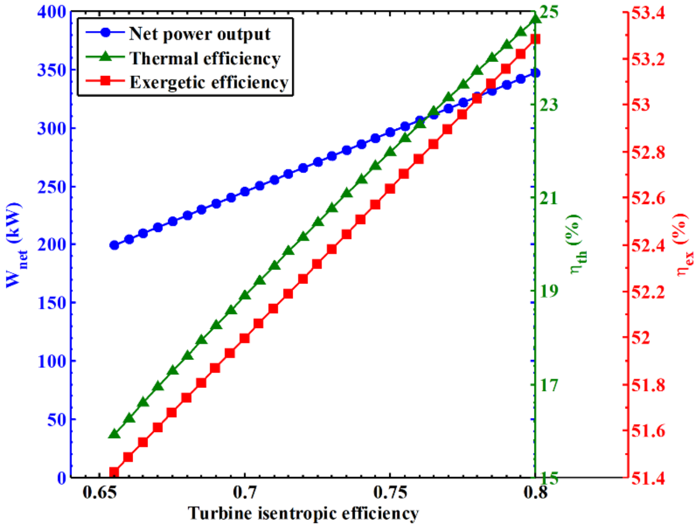

Fig. 10. Variations in system net power output, thermal efficiency and exergetic efficiency with turbine isentropic efficiency.

4.1.6. Effects of the turbine inlet temperature

The maximum temperature of the whole system is the outlet temperature of the gas heat exchanger which is also equal to the turbine inlet temperature. In Fig.11, the system net power output, thermal efficiency and exergetic efficiency all increase almost proportionally to the increase of the turbine inlet temperature. The increase in the turbine inlet temperature by 50 ℃ results in an increase in the net power output, thermal efficiency and exergetic efficiency by approximately 18%, 14% and 2.0%, respectively. It is clear that increasing the turbine inlet temperature is the most straightforward way to improve the system performance, and this confirms that the S-CO_2 recompression Brayton power cycle is suitable for exploiting the high-temperature heat source. In this study, the turbine inlet design temperature is about 420 ℃ based on the ship main engine exhaust gas maximum temperature (460 ℃).

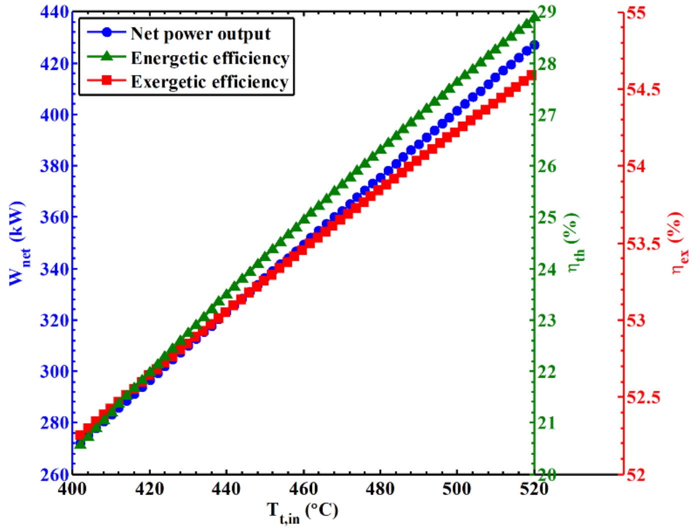

Fig. 11. Variations in system net power output, thermal efficiency and exergetic efficiency with turbine inlet temperature.

According to the results of thermodynamic analysis, values of the thermodynamic parameters to conduct the following performance multi-objective optimizations are listed in Table 6.

Table 6

Thermodynamic parameters for performance multi-objective optimization.

Parameters	Values
Main compressor inlet temperature (℃)	34
Main compressor inlet pressure (MPa)	8.0
Pressure ratio	2.5
Turbine inlet temperature (℃)	420
Turbine isentropic efficiency (%)	75
Re-compressor isentropic efficiency (%)	65
Main compressor isentropic efficiency (%)	65

4.2. Multi-objective optimization

For a thermodynamic system like the S-CO_2 cycle, system performance optimization can involve two or more conflicting objectives. The multi-objective optimization provides an effective method by which such issues may be resolved, but the issue that must be addressed is that it is difficult to get a feasible solution when the maximization and minimization objective is conflicted during the calculation process of the multi-objective optimization, especially since both objectives are indispensable considerations (Li et al. 2015). In this work, NSGA-II is used to get the Pareto front solutions of the objective functions, then LINMAP and TOPSIS decision-making methods are employed to determine the final optimal result from the Pareto front solutions.

4.2.1. Problem formulation

The purpose of system performance multi-objective optimization is to maximize net power output W_{net} and exergetic efficiency η_{ex} as well as to minimize the levelized cost of energy *LCOE* by investigating the decision variables of flow split ratio *x*, mass flow rate m_{t} and exhaust gas waste heat temperature T_{g}. The multi-objective optimization model is established according to the proposed system energetic, exergetic and economics models described in Section 2, which can be expressed as follows:

$$\begin{cases} \max\ f_1(m_{\mathrm{t}}, x, T_g) = W_{\mathrm{net}} \\ \max\ f_2(m_{\mathrm{t}}, x, T_g) = \eta_{\mathrm{ex}} \\ \min\ f_3(m_{\mathrm{t}}, x, T_g) = LCOE \end{cases} \tag{20}$$

According to the working principle of the S-CO_2 RBC, the flow split ratio x is defined as the proportion of the working fluid's mass flow rate into the recompression compressor divided by the total working fluid's mass flow rate, and ranges from 0 to 1.0 for this study. The design net power output of the proposed system is 300 kW, based on an estimation that the mass flow rate m_{t} ranges from 10.0 kg/s to 12.0 kg/s. Based on the ship main engine working conditions, the temperature range of the exhaust gas waste heat T_{g} is 400 ℃ to 460 ℃.

4.2.2. Optimization results and discussions

Fig.12 shows the Pareto front solutions and the final optimal results decided by LINMAP and TOPSIS decision-making methods of the triple-objective ($W_{\mathrm{net}} - LCOE - \eta_{\mathrm{ex}}$) optimization. As can be seen the *LCOE* increases with the increase of net power output and exergetic efficiency. The optimal solutions for the net power output, exergetic efficiency and levelized cost of energy are within the ranges of 107.50 kW to 313.30 kW, 13.40% to 40.19% and 0.01 $/kWh to 0.03 $/kWh, respectively. Table 7 lists the final optimal results of the triple-objective optimization determined by LINMAP and TOPSIS decision makings in detail. It is observed that the final optimal solutions always occur at the upper limit of the heat source temperature, which indicates that higher exhaust gas temperatures have a positive effect on the system performance. The final optimal result deviation index for the triple-objective optimization obtained by TOPSIS (0.2517) is less than that of LINMAP (0.1997). Therefore, the final optimal result decided by the TOPSIS decision making is deemed as being more realistic in the triple-objective optimization. To reveal the relationship between the three objectives, the mathematical expression obtained by fitting the Pareto front solution is given by:

$$LCOE = -68.14 \cdot W_{\mathrm{net}}^2 - 0.29 \cdot W_{\mathrm{net}} - 40.77 \cdot \eta_{\mathrm{ex}}^2 + 0.11 \cdot \eta_{\mathrm{ex}} + 105.80 \cdot W_{\mathrm{net}} \cdot \eta_{\mathrm{ex}} + 0.02 \tag{21}$$

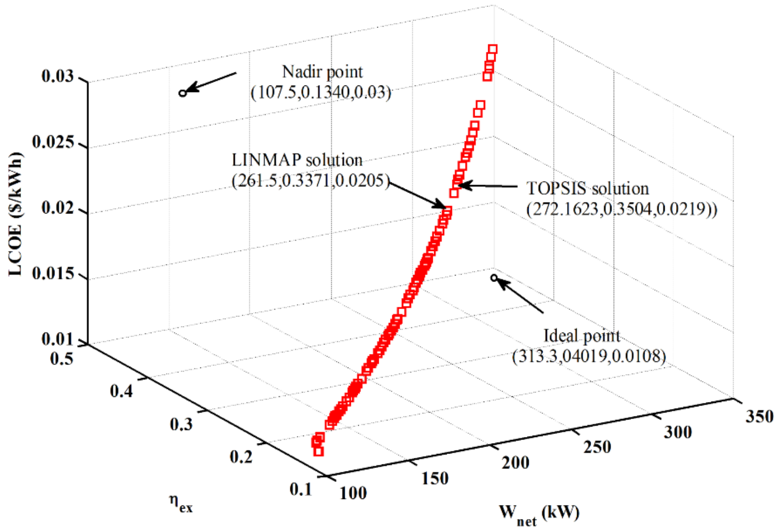

Fig.12. The pareto front curve of triple-objective for the presented system.

Table 7

Multi-objective optimization results by using LINMAP and TOPSIS decision makings.

Parameters	Ideal point	Nadir point	LINMAP	TOPSIS
W_{net} (kW)	313.30	107.50	261.50	272.20
η_{ex} (%)	40.19	13.40	33.71	35.04
LCOE ($/kWh)	0.0108	0.0300	0.0205	0.0219
x	0.99	0.10	0.67	0.72
m_t (kg/s)	11.99	12.00	11.99	12.00
T_g (K)	733.05	732.79	732.76	732.53
Deviation index			0.2517	0.1997

Three 2D figures detailing the Pareto front solutions and curve fitting for dual-objective ($W_{net}-LCOE$, $\eta_{ex}-LCOE$, $W_{net}-\eta_{ex}$) optimizations are shown in Fig.13 which provide better understanding of the relationships between net power output, exergetic efficiency and levelized cost of energy. As can be seen from Fig.13 (a), the levelized cost of energy increases with the increase of net power output. Under the given conditions, the proposed system can deliver a maximum net power output of 313.30 kW with a maximum levelized cost of energy of 0.03 $/kWh. The relationship between these two objectives is expressed as:

$$LCOE_{W_{net}} = 11 \cdot W_{net}^4 - 7.2 \cdot W_{net}^3 + 1.9 \cdot W_{net}^2 - 0.19 \cdot W_{net} + 0.017 \tag{22}$$

The increase of exergetic efficiency leads to an increase in the levelized cost of energy as shown in Fig. 13 (b). Fig.13 (c) shows that the exergetic efficiency increases linearly with the increase of net power output. The mathematical expressions to describe the relationships between levelized cost of energy and exergetic efficiency, exergetic efficiency and net power output are given as follows:

$$LCOE_{\eta_{ex}} = 4.9 \cdot \eta_{ex}^4 - 4.3 \cdot \eta_{ex}^3 + 1.5 \cdot \eta_{ex}^2 - 0.21 \cdot \eta_{ex} + 0.021 \tag{23}$$

$$\eta_{ex} = 1.3 \cdot W_{net} + 0.0092 \tag{24}$$

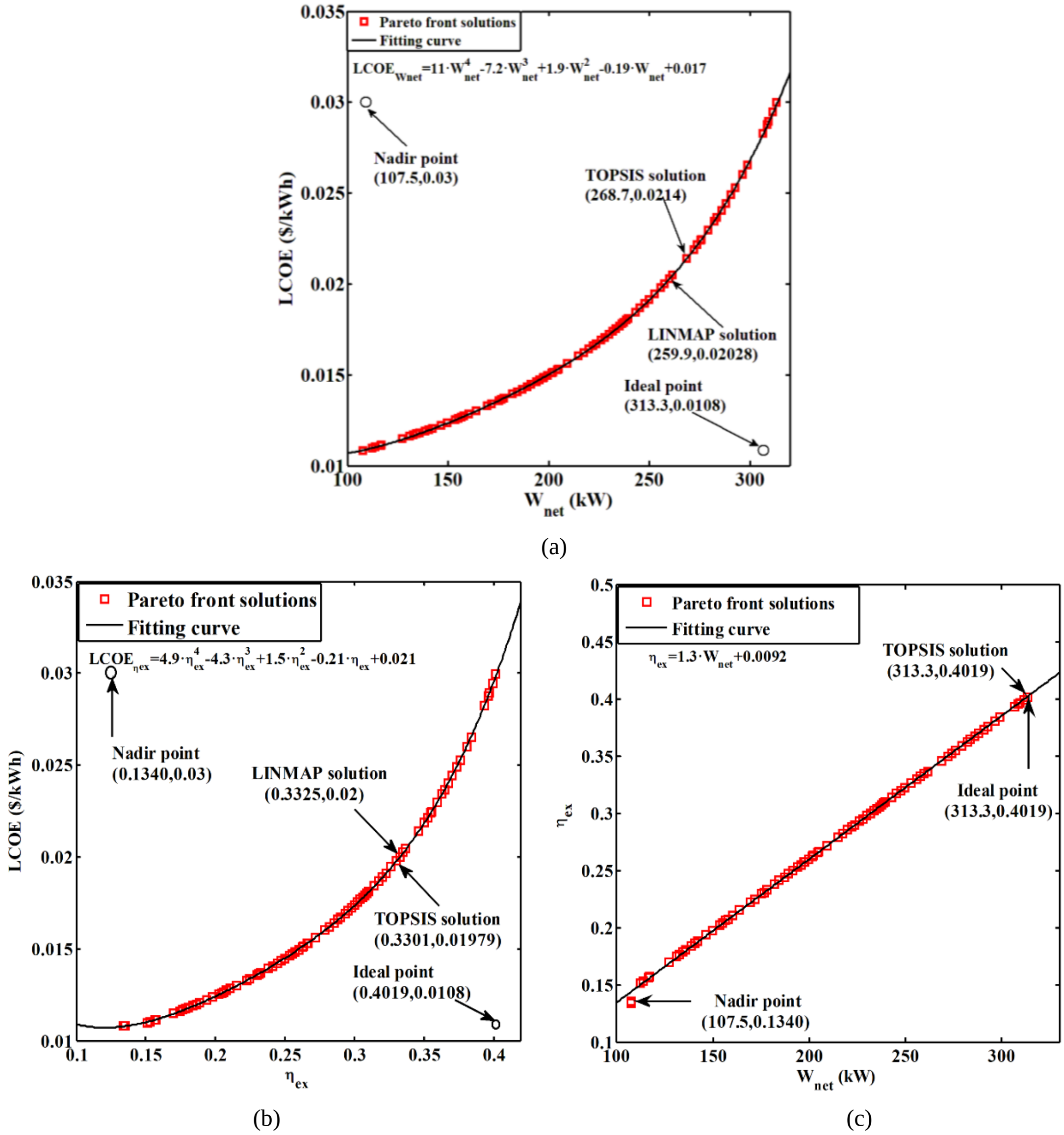

Fig.13. Pareto front solutions fitting curves: (a). Net power output and levelized cost of energy; (b). Exergetic efficiency and levelized cost of energy; (c). Net power output and exergetic efficiency.

The final optimal results for these dual-objective optimizations decided by LINMAP and TOPSIS decision makings as well as their deviation indexes are listed in Tables 8 to 10. In Table 8, the deviation index for the final optimal result decided by TOPSIS (0.2167) is less than that from LINMAP (0.2595), which is consistent with the result in the triple-objective optimization decision making processes. The deviation index for the final optimal result decided by the TOPSIS (0.2693) in Table 9 is higher than that from LINMAP (0.2605). The inconsistency of the deviation index in Table 9 with that in Table 7 and Table 8 indicates that there is no clear standard to decide which method is suitable to conduct the multi-objective decision making for the S-CO_2 RBC system performance. However, by comprehensively comparing the optimization results, TOPSIS decision making is deemed the better choice to determine the final optimal result in this research project. Owing to the linear relationship between net power output and exergetic efficiency, the final optimal result of the dual-objective ($W_{net} - \eta_{ex}$) is obtained at the ideal point, at which the deviation index is 0 (Table 10). By analyzing the final optimal results of the multi-objective optimizations, the deviation indexes of the final optimal results decided by TOPSIS and LINMAP methods for dual-objective optimizations are higher than that of the triple-objective optimization. In addition, the final optimal net power output and exergetic efficiency decided by the TOPSIS decision making in the triple-objective optimization are higher than those calculated by the dual-objective optimizations by approximately 1.29% and 5.11%, and the levelized cost of energy calculated by the dual-objective optimization is 2.28% lower than that of the triple-objective optimization. In summary, triple-objective optimization can produce more reliable optimization results than dual-objective or even single-objective optimization.

Table 8

Comparison between optimal solutions for dual-objective (W_{net}-*LCOE*) optimization.

	Decision makings	Design variables			Objectives		Deviation index
		x	m_t (kg/s)	T_g (K)	W_{net} (kW)	*LCOE* ($/kWh)	
NSGA-II	LINMAP	0.67	11.99	732.76	259.90	0.0203	0.2595
	TOPSIS	0.70	11.99	733.15	268.70	0.0214	0.2167

Table 9

Comparison between optimal solutions for dual-objective (η_{ex} -*LCOE*) optimization.

	Decision makings	Design variables			Objectives		Deviation index
		x	m_t (kg/s)	T_g (K)	η_{ex} (%)	*LCOE* ($/kWh)	
NSGA-II	LINMAP	0.68	11.99	733.12	33.25	0.0200	0.2605
	TOPSIS	0.66	12.00	733.14	33.01	0.0190	0.2693

Table 10

Comparison between optimal solutions for dual-objective (W_{net}-η_{ex}) optimization.

	Decision makings	Design variables			Objectives		Deviation index
		x	m_t (kg/s)	T_g (K)	W_{net} (kW)	η_{ex} (%)	
NSGA-II	LINMAP						
	TOPSIS	0.99	11.99	733.05	313.30	40.19	0

The effects on the three objective functions by flow split ratio and mass flow rate as decision variables were analyzed. The contour plots in Fig. 14 show the variations of W_{net}, η_{ex} and *LCOE* along with flow split ratio x and mass flow rate m_t. As can be seen from the contour plot in Fig. 14 (a), the maximum net power output is obtained close to the upper limit of the flow split ratio. According to the definition of flow split ratio, it indicates that as more working fluid CO_2 flows into the re-compressor it produces more power from the proposed system. It is clear that the recompression cycle has the ability to produce more power than that of the simple recuperated cycle without recompression (x=0). The effects of flow split ratio and mass flow rate on the exergetic efficiency and levelized cost of energy are shown in Fig. 14 (b) and Fig. 14 (c), respectively. From Fig. 14 (b), the peak exergetic efficiency occurs at the upper limit of the flow split ratio. That is because the heat energy in the working fluid can be further exploited in the recompression loop instead of being released to the environment through the pre-cooler, which can more fully exploit the waste heat to reduce the exergy loss and improve system exergetic efficiency. Therefore, compared with the simple recuperated cycle without recompression, the recompression Brayton cycle can improve the utilization of the waste heat. As can be seen from Fig. 14 (c), it is much more economic for the recompression Brayton cycle if it has a higher flow split ratio. Since the recompression Brayton cycle produces more power, this results in decrease of the levelized cost of energy. Compared with the simple recuperated cycle without recompression, the recompression Brayton cycle has advantages in system net power output, exergetic efficiency and levelized cost of energy. Considering the system performance and economics simultaneously, the recompression Brayton cycle is a better choice to exploit the ship's main engine exhaust gas waste heat recovery for this research project.

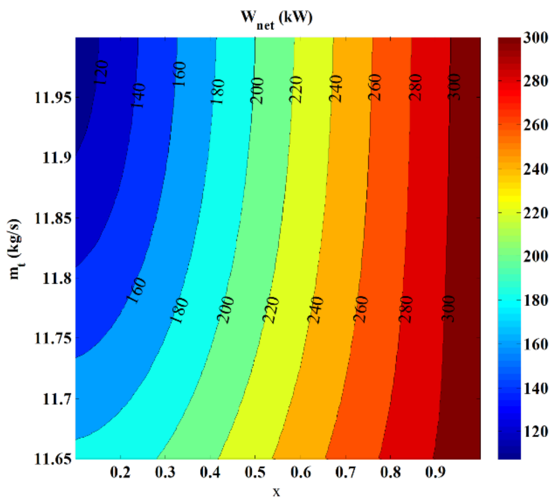

(a)

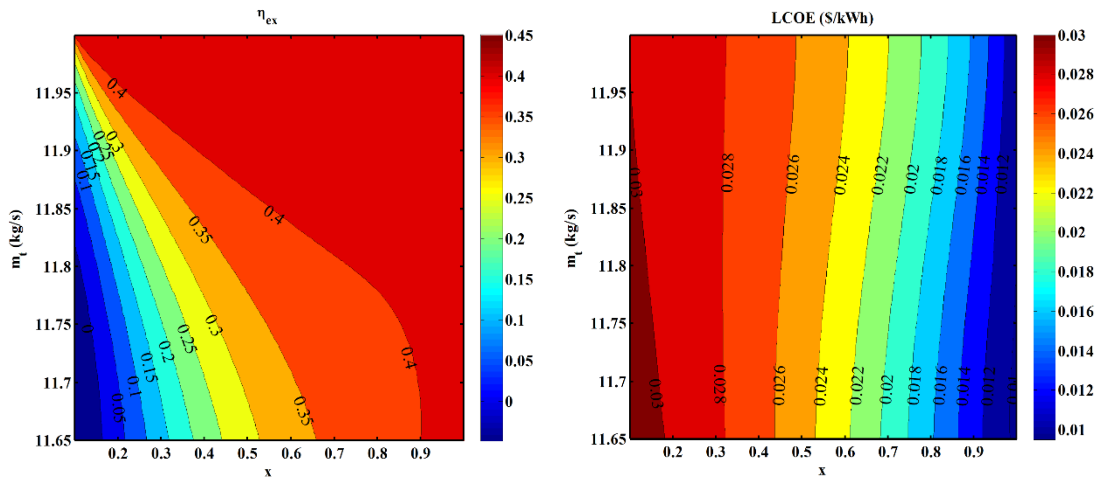

(b) (c)

Fig.14. Objectives variations with mass flow rate and flow split ratio: (a). Net power output; (b). Exergetic efficiency; (c). Levelized cost of energy.

5. Conclusions

The thermodynamic models of the S-CO_2 recompression Brayton cycle for recovering the main engine exhaust gas waste heat from an ocean-going 9000 TEU container ship are established to evaluate the potential performance from both thermodynamic and economic perspectives by thermodynamic analysis and multi-objective optimization. A theoretical analysis is conducted to determine the effects of thermodynamic parameters on the steady-state system performance and decide their initial values, including main compressor inlet temperature, main compressor inlet pressure, pressure ratio, turbine inlet temperature and turbomachinery isentropic efficiency. For the purpose of maximizing the net power output and exergetic efficiency as well as minimizing the levelized cost of energy triple-objective ($W_{net}-\eta_{ex}-LCOE$) and dual-objective ($W_{net}-\eta_{ex}$, $\eta_{ex}-LCOE$, $W_{net}-LCOE$) optimizations were conducted using the NSGA-II algorithm-based multi-objective optimization, where flow split ratio, mass flow rate and exhaust gas waste heat temperature were considered as decision variables. To determine the final optimal result from Pareto front solutions, LINMAP and TOPSIS decision-making methods were employed. The main conclusions were as follows:

(1) The results of the thermodynamic analysis reveal that the thermodynamic parameters have significant and comprehensive effects on the system's overall performance. Specifically, higher main compressor inlet temperature has a negative effect on system performance. The proposed system achieved better system performance at the relatively low main compressor inlet temperature of approximately 34 ℃. The main compressor

inlet pressure brings positive effects on the system exergetic efficiency, while its effect on the system's net power output is no longer so significant when it exceeds 8.0 MPa. When the pressure ratio is in the range of 2.0 ~ 3.0, there is a positive effect on the system net power output and exergetic efficiency, but the net power output and exergetic efficiency all have their own optimal pressure ratios. Higher turbomachinery isentropic efficiency contributes to better system performance, but such benefits will be restricted by the manufacturing technologies. So, on the basis of the thermodynamic analysis, the initial thermodynamic parameters are fixed at $T_{\mathrm{mc,in}}$ =34 ℃, $P_{\mathrm{mc,in}}$ =8.0 MPa, P_r =2.5, $isen_{\mathrm{mc}}$ =0.65 and $isen_{\mathrm{t}}$ =0.75.

(2) The Pareto front results showed that the levelized cost of energy increased with the increase of net power output and exergetic efficiency, which were in the ranges of 0.01 $/kWh to 0.03 $/kWh, 107.50 kW to 313.30 kW and 13.40% to 40.19%, respectively. The maximized system performance solution occurs close to the upper limit of the exhaust gas waste heat temperature, which indicates that higher exhaust gas waste heat temperature can produce a positive effect on the system performance. In addition, the curve fits and mathematical expressions to demonstrate the relationships between the objective functions based on Pareto front solutions were plotted and obtained, which could be used to assist the S-CO_2 recompression Brayton cycle waste heat recovery system's optimal design.

(3) By comparing the deviation indexes of the final optimal results decided by LINMAP and TOPSIS decision-making methods, the TOPSIS decision making was deemed the reasonable choice. In addition, the final optimal net power output and exergetic efficiency obtained by triple-objective optimization were higher than the results calculated by dual-objective optimizations by 1.29% and 5.11%, while the levelized cost of energy calculated by dual-objective optimization was 2.28% lower than that from the triple-objective. Therefore, the triple-objective optimization provided more reasonable results than that from dual-objective optimization or even single-objective optimization.

(4) The results of the flow split ratio and mass flow rate effects on the net power output, exergetic efficiency and levelized cost of energy confirmed that the recompression Brayton cycle is an acceptable choice to be used to recover the ship main engine exhaust gas waste heat compared with the simple recuperated cycle without recompression.

(5) In this study, the working fluid CO_2 in the system is considered to be always in the supercritical state. However, considering that when the system is shut down and restarted, some of the remaining working fluid CO_2 in the system may not be in its

supercritical state. Thus, the influence of the transcritical CO_2 on performance of S-CO_2 recompression Brayton cycle system needs to be further studied.

Declaration of Competing Interest

The authors declare that they have no known competing financial interests or personal relationships that could have appeared to influence the work reported in this paper.

Acknowledgements

This work was supported by the High-Tech Ship Research Project of Ministry of Industry and Information Technology, P. R. China (No. MIIT [2017] 614). In addition, many thanks to Mr. Konrad Yearwood at the Department of Mechanical Engineering, University College London (UCL), for his helpful suggestions and comments to improve the quality of this paper.

Biography

Pengcheng PAN, PhD student. Research interests: green ship and S-CO_2 waste heat recovery for ship use.

Professor, Chengqing YUAN. Research interests: renewable energy application technology.

Associate Professor, Yuwei SUN. Research interests: renewable energy application technology, electric power system and automation, system modeling and simulation

References

Akbari AD, Mahmoudi SMS. 2014. Thermoeconomic analysis & optimization of the combined supercritical CO_2 (carbon dioxide) recompression Brayton/organic Rankine cycle. Energy 78: 501-12.

Al-Sulaiman F, Atif M. 2015. Performance comparison of different supercritical carbon dioxide Brayton cycles integrated with a solar power tower. Energy 82: 61-71.

Angelino G. 1968. “Carbon Dioxide Condensation Cycles for Power Production,” ASME J Eng Gas Turbines Power 3: 287–95.

Banik S, Ray S, De S. 2016. Thermodynamic modelling of a recompression CO_2 power cycle for low temperature waste heat recovery. Appl Therm Eng 107: 441-52.

Bella DFA. 2015. Gas turbine engine exhaust waste heat recovery using supercritical CO_2 Brayton cycle with thermoelectric generator technology, in: ASME, 9th International Conference of Energy Sustainability, 28th Jun-2nd Jul, 2015, V001T04A003.

Belmonte MAR, Sebastián A, Romero M, Aguilar JG. 2016. Optimization of a recompression supercritical carbon dioxide cycle for an innovative central receiver solar power plant. Energy 112: 17-27.

Beşikci EB, Arslan O, Turan O, Ölcer AI. 2016. An artificial neural network based decision support system for energy efficient ship operations. Comput Oper Res 66: 393-401.

Binotti M, Astolfi M, Campanari S, Manzolini G, Silva P. 2017. Preliminary assessment of S-CO_2 power cycles for application to CSP solar tower plants. The 8th International Conference on Applied Energy- ICAE2016. Energy Procedia 105: 1116-22.

Cao Y, Ren JQ, Sang YQ, Dai YP. 2017. Thermodynamic analysis and optimization of a gas turbine and cascade CO_2 combined cycle. Energ Convers Manage 144: 193-204.

Cheng WL, Huang WX, Nian YL. 2017. Global parameter optimization and criterion formula of supercritical carbon dioxide Brayton cycle with recompression. Energ Convers Manage 150: 669-77.

Choi BC. 2016. Thermodynamic analysis of a transcritical CO_2 heat recovery system with 2-stage reheat applied to cooling water of internal combustion engine for propulsion of the 6800 TEU container ship. Energy 107: 532-41.

Crespi F, Gavagnin G, Sánchez D, Martínez GS. 2017. Supercritical carbon dioxide cycles for power generation: A review. Appl Energ 195: 152-83.

Crespi F, Sánchez D, Rodríguez JM, Gavagnin G. 2017. Fundamental thermo-Economic approach to selecting S-CO_2 power cycle for CSP applications. IV International Seminar on ORC Power Systems, ORC 2017 13-15 September 2017, Milano, Italy. Energy Procedia 129: 963-70.

Deb K, Pratap A, Agarwal S, Meyarivan T. 2002 A fast and elitist multi-objective genetic algorithm: NSGA-II. IEEE Trans Evol Comput 6: 182-97.

Deng QH, Wang D, Zhao H, Huang WT, Shao S, Feng ZP. 2017. Study on performances of supercritical CO_2 recompression Brayton cycles with multi-objective optimization. Appl Therm Eng 114: 1335-42.

Dostal V, Driscoll MJ, Hejzlar P. 2004. A supercritical carbon dioxide cycle for next generation nuclear reactors. Advanced nuclear power technology program.

Dostal V. 2004. A supercritical carbon dioxide cycle for next generation nuclear reactors [Ph.d. Thesis]. USA: Massachusetts Institute of Technology.

Dyreby JJ. 2014. Modeling the Supercritical Carbon Dioxide Brayton Cycle with Recompression. [Ph.d. Thesis]. USA: University of Wisconsin-Madison.

Feher EG. 1968. “The Supercritical Thermodynamic Power Cycle,” Energy Convers 2: 85–90.

Guo ZP, Zhao Y, Zhu YX, Niu FL, Lu DG. 2018. Optimal design of supercritical CO_2 power cycle for next generation nuclear power conversion systems. Prog Nucl Energ 108:111-21.

Hou SY, Wu YD, Zhou YD, Yu LJ. 2017. Performance analysis of the combined supercritical CO_2 recompression and regenerative cycle used in waste heat recovery of marine gas turbine. Energ Convers Manage 151: 73-85.

Hwang CL, Yoon KP. 1981. Multiple attribute decision making: Methods and applications. Springer-Verlag.

Kulhánek M, Dostál V. 2011. Supercritical carbon dioxide cycles thermodynamic analysis and comparison. In: Supercritical CO_2 power cycle symposium, Boulder, CO.

Lee KJ, Shin DS, Yoo DW, Choi HK, Kim HJ. 2013. Hybrid photovoltaic/diesel green ship operating in standalone and grid-connected mode-Experimental investigation. Energy 49: 475-83.

Li MJ, Zhu HH, Guo JQ, Wang K, Tao WQ. 2017. The development technology and applications of supercritical CO_2 power cycle in nuclear energy, solar energy and other energy industries. Appl Therm Eng 126: 255-75.

Li YQ, Liao SM, Liu G. 2015. Thermo-economic multi-objective optimization for a solar-dish

Brayton system using NSGA-II and decision making. Int J Elec Power 64:167-175.

Liu M, Zhang XW, Ma YG, Yan JJ. 2018. Thermo-economic analysis on a new conceptual system of waste heat recovery integrated with an S-CO_2 cycle for coal-fired power plants. Energ Convers Manage 161: 243-253.

Manente G, Fortuna FM. 2019. Supercritical CO_2 power cycles for waste heat recovery: A systematic comparison between traditional and novel layouts with dual expansion. Energ Convers Manage 197:111777.

Moghimi M, Emadi M, Ahmadi P, Moghadasi H. 2018. 4E analysis and multi-objective optimization of a CCHP cycle based on gas turbine and ejector refrigeration. Appl Therm Eng 141: 516-30.

Moroz L, Burlaka M, Rudenko O, Joly C. 2015. Evaluation of gas turbine exhaust heat recovery utilizing composite supercritical CO2 cycle, in: Proceedings of International Gas Turbine Congress, Tokyo, Japan, 15th-20th Nov 2015, ISBN978-4-89111-008-6.

NIST Standard Reference Database 23. 2013. NIST thermodynamic and transport properties of refrigerants and refrigerant mixtures REFPROP, Version 9.1.

Park JH, Park HS, Kwon JG, Kim TH, Kim MH. 2018. Optimization and thermodynamic analysis of supercritical CO_2 Brayton recompression cycle for various small modular reactors. Energy 160: 520-35.

Perera LP, Mo B. 2016. Emission control based energy efficiency measures in ship operations. Appl Ocean Res 60: 29-46.

Polimeni S, Binotti M, Moretti L, Manzolini G. 2018. Comparison of sodium and KCl-MGCl2 as heat transfer fluids in CSP tower with S-CO_2 power cycles. Sol Energy 162: 510-24.

Poulsen RT, Johnson H. 2016. The logic of business vs. the logic of energy management practice: understanding the choices and effects of energy consumption monitoring systems in shipping companies. J Clean Prod 112: 3785-97.

Sarkar J, Bhattacharyya S. 2009. Optimization of recompression S-CO_2 power cycle with reheating. Energ Convers Manage 50: 1939-45.

Sarkar J. 2009. Second law analysis of supercritical CO_2 recompression Brayton cycle. Energy 34: 1172-8.

Sharma OP, Kaushik SC, Manjunath K. 2017. Thermodynamic analysis and optimization of a supercritical CO_2 regenerative recompression Brayton cycle coupled with a marine gas turbine for shipboard waste heat recovery. Therm Sci Eng Prog 3: 62-74.

Shi Y, Reitz RD. 2010. Assessment of multi-objective genetic algorithms with different niching strategies and regression methods for engine optimization and design. J Eng Gas Turbines

Power 132: 052801.

Shu GQ, Liu P, Tian H. 2017. Operational profile based thermal-economic analysis on an Organic Rankine cycle using for harvesting marine engine's exhaust waste heat. Energ Convers Manage 146: 107-23.

Sianaki OA. 2015. Intelligent decision support system for energy management in demand response programs and residential and industrial sectors of the smart grid. [Ph.d. Thesis]. Australia: Curtin University.

Singh DV, Pedersen E. 2016. A review of waste heat recovery technologies for maritime applications. Energ Convers Manage 111: 315-28.

Sulzer G. Verfahren zur erzeugung von arbeit aus warme, Swiss Patent; 1950. 269599.

Tian H, Chang LW, Shu GQ, Shi LF. 2017. Multi-objective optimization of the carbon dioxide transcritical power cycle with various configurations for engine waste heat recovery. Energ Convers Manage 148: 477-88.

Wang JF, Sun ZX, Dai YP, Ma SL. 2010. Parametric optimization design for supercritical CO_2 power cycle using genetic algorithm and artificial neural network. Appl Energ 87: 317-24.

Wu C, Wang SS, Feng XJ, Li J. 2017. Energy, exergy and exergoeconomic analysis of a combined supercritical CO_2 recompression Brayton/absorption refrigeration cycle. Energ Convers Manage 148: 360-77.

Yoon YS, Kim MJ, Kim IS, Kim TS. 2017. Comparison of micro gas turbine heat recovery systems using ORC and trans-critical CO_2 cycle focusing on off-design performance. IV International Seminar on ORC Power Systems, ORC 2017 13-15 September 2017, Milano, Italy. Energy Procedia 129: 987-94.

Yuan CQ, Pan PC, Sun YW, Yan XP, Tang XJ. 2019. The evaluating on EEDI and fuel consumption of an inland river 800PCC integrated with solar photovoltaic system. J Mar Eng Technol.

Yuan CQ, Pan PC, Sun YW, Yan XP, Zhang Y, Tang XJ. 2018. Attained EEDI and fuel consumption of ships with integrated and high-efficiency heat power generation systems. Shipbuilding of China 1: 195-206.

Zhang Q, Ogren RM, Kong SC. 2018. Thermo-economic analysis and multi-objective optimization of a novel waste heat recovery system with a transcritical CO_2 cycle for offshore gas turbine application. Energ Convers Manage 172: 212-27.

Zhao H, Deng QH, Huang WT. 2016. Thermodynamic and economic analysis and multi-objective optimization of supercritical CO_2 Brayton cycles. J Eng Gas Turbines Power 138: 1602-9.